A Survey of Anticyclonic Mesoscale Eddies, Within the Southern Ocean, and their Propagation South From the South West Indian Ridge

Kirrin Gail Reid
RDXKIR002

Thesis submitted in partial fulfilment of the requirements for the degree of Master of Science in Ocean & Climate Dynamics

Department of Oceanography, University of Cape Town
February 2016

Supervisor: Isabelle Ansorge

The copyright of this thesis vests in the author. No quotation from it or information derived from it is to be published without full acknowledgement of the source. The thesis is to be used for private study or non-commercial research purposes only.

Published by the University of Cape Town (UCT) in terms of the non-exclusive license granted to UCT by the author.

University of Cape Town

PLAGIARISM DECLARATION

COURSE NAME: Master of Science in Ocean & Climate Dynamics
COURSE CODE: SEA5010W
STUDENT NAME: Kirrin Gail Reid
STUDENT NUMBER: RDXKIR002

- I know the meaning of plagiarism and declare that all of the work in this document, save for that which is properly acknowledged, is my own
- I understand that plagiarism is a serious form of academic dishonesty. Plagiarism is to use another's work and claim it to be your own work
- Each significant contribution to, and quotation in this paper from, the work or works of other people has been cited and referenced in the APA referencing format.
- I declare that this paper is my own work
- I have not allowed, and will not allow, anyone to copy my work

SIGNATURE: Signed by candidate

Signature removed

Kirrin Reid

DATE: 15/02/2016

ACKNOWLEDGEMENTS

Thanks go to Captain Mr Gavin Syndercombe, the officers and the crew aboard the SA Agulhas II during the 2014 Marion Island Relief Cruise [MIRC2014], without whom this survey would not have been possible. I'd like to also thank A/Prof Isabelle Ansorge, Mr Gavin Tut, Mr Marcel Van Den Berg and my fellow University of Cape Town [UCT] Oceanography students who helped with data capture and processing during the MIRC2014. Many thanks too, to Isabelle, my supervisor, for all the help, advice, guidance and support. I am grateful to the National Research Foundation [NRF] and the University of Cape Town [UCT], through their SANAP programme, for providing funding towards my Master's years in Ocean & Climate Dynamics.

The financial assistance of UCT and the NRF towards this research is hereby acknowledged. Opinions expressed, and conclusions arrived at, are those of the author and not necessarily to be attributed to either the NRF or UCT.

ABSTRACT

Eddies within oceans act as vehicles, transporting smaller bodies of water, with certain oceanographic characteristics, from one place to another within a larger body of water. The South West Indian Ridge [SWIR] is a topographically complex bathymetric feature which amplifies the production of mesoscale eddies in and around the Antarctic Circumpolar Current [ACC]. Within the Southern Ocean [SO], a section of this ridge - the Andrew Bain Fracture Zone [ABFZ] - has been found to be the starting line of an eastward extending eddy corridor. Earlier research shows an area of diminishing mesoscale variability within this corridor which extends down from 45°S to approximately 60°S. A recent study focused on a southward extending anticyclonic eddy corridor and proved its existence. The anticyclonic [warm core] eddies which are propagating south, not previously investigated through in situ means, were observed during the 2014 Marion Island Relief Cruise [MIRC2014] aboard the SA Agulhas II. Two anticyclonic mesoscale eddies [one juvenile and one mature] were bisected with transects of conductivity, temperature and depth stations and expendable bathythermograph deployments. This paper used the in situ data captured during the MIRC2014 to study the internal structure of the two eddies. The objectives of this study were also to examine both the recent and the historical trajectory characteristics of the southward advecting anticyclonic eddies, to confirm the origin of the two sampled eddies, and to assess the structural differences between the two anticyclonic eddies. This paper plots the behaviour of the anticyclonic mesoscale eddies found within the area of the southward eddy corridor, firstly using website available data collected over a two year period [May 2012 – May 2014] and then utilizing a previously compiled data set to plot the historical dynamics [October 1992 – April 2012]. The trajectories of the southward anticyclones during that time period were found to be predominantly southward, typically following the south west slope of the SWIR. The two MIRC2014 eddies were confirmed to originate from the ABFZ section of the SWIR. Each eddy had a similar grouping of water masses; Antarctic Bottom Water, Circumpolar Deep Water, Antarctic Intermediate Water, Winter Water and Sub-Antarctic Surface Water: water masses characteristic of the Antarctic Polar Frontal Zone [APFZ]. The in situ measurement and analysis of these eddies allowed the first comparison between a juvenile and a mature anticyclonic eddy in the recently discovered southward extending eddy corridor. Thermal section comparisons of these two sampled anticyclonic eddies showed that, over time, these anticyclonic eddies appear to shrink in surface diameter, deepen and lose heat to host waters. This loss of heat occurs due to the degradation of water mass boundary integrity over time and is theorised to accelerate as time passes. This study shows that the southward extending eddy corridor is a means of shifting heat and salt further south within the SO, large sections of which are sink areas for atmospheric CO_2. This poleward heat transport influences the capability of the SO to absorb atmospheric CO_2, since higher temperatures negatively affect the ocean's CO_2 uptake capability. The results of this study are proposed to be a catalyst for future in situ sampling across eddies in this area, in order that heat and salt transport, through this southward anticyclonic eddy corridor, can be monitored for fluctuations. As this carbon sink is vitally important with regards to climate change, the quantification of the heat and salt sources of the SO, which alter the SO's ability to absorb CO_2, is imperative.

LIST OF CONTENTS Page

LIST OF TABLES & FIGURES: Page

1 - LITERATURE REVIEW

1.1 - AN OVERVIEW OF THE SOUTHERN OCEAN

The region of the globe's ocean lying south of 40°S is known as the Southern Ocean [SO] and covers over 25% of the global ocean surface area. Rintoul and Naveira Garabato (2013) stated that the SO is the only region of the global ocean where deep waters upwell to the surface allowing for the exchange of Carbon Dioxide [CO_2] with the atmosphere. As a direct consequence of the Southern Ocean's extensive domain, and the availability of air-sea interactions between sub-polar and sub-tropical regions, the SO plays an important role in shaping the global climate (White and Peterson, 1996).

The Antarctic continent marks the southern boundary of the SO, but the northern 'boundary' is not well defined. The Antarctic Treaty's political limit at 60°S could be taken as the northern limit. However oceanographically, the Southern Ocean's regime extends well north of 60°S, due to the strong wind forcing and oceanographic circulation which occurs within the global ocean. The annual mean wind forcing for the SO is controlled by westerlies, between 30-65˚S, and also by easterlies, south of 60°S (Talley, 2011).

The SO is strongly connected to its three northern counterparts; the Atlantic, the Indian and the Pacific Oceans. Climatic and oceanic signals, which occur in one region of the globe, can therefore be transported basin-wide to another part of the world's ocean via the Southern Ocean pathway (Gille, 2002; Iudicone et al., 2008). This inter-basin connection allows the formation of a global-scale overturning circulation: the Meridional Overturning Circulation [MOC; Figure 1]. The MOC is a global network of typically density-driven ocean currents consisting of both surface currents and mid-to-deep under-currents (Sloyan and Rintoul, 2001). The MOC allows for the transport of heat, salt, carbon dioxide and other biogeochemical properties from one ocean basin to the other (Sloyan and Rintoul, 2001). Thus the circulation of the SO, a significant limb of the MOC, has important implications for the global ocean circulation and strongly influences the Earth's regional and global climate (White and Peterson, 1996).

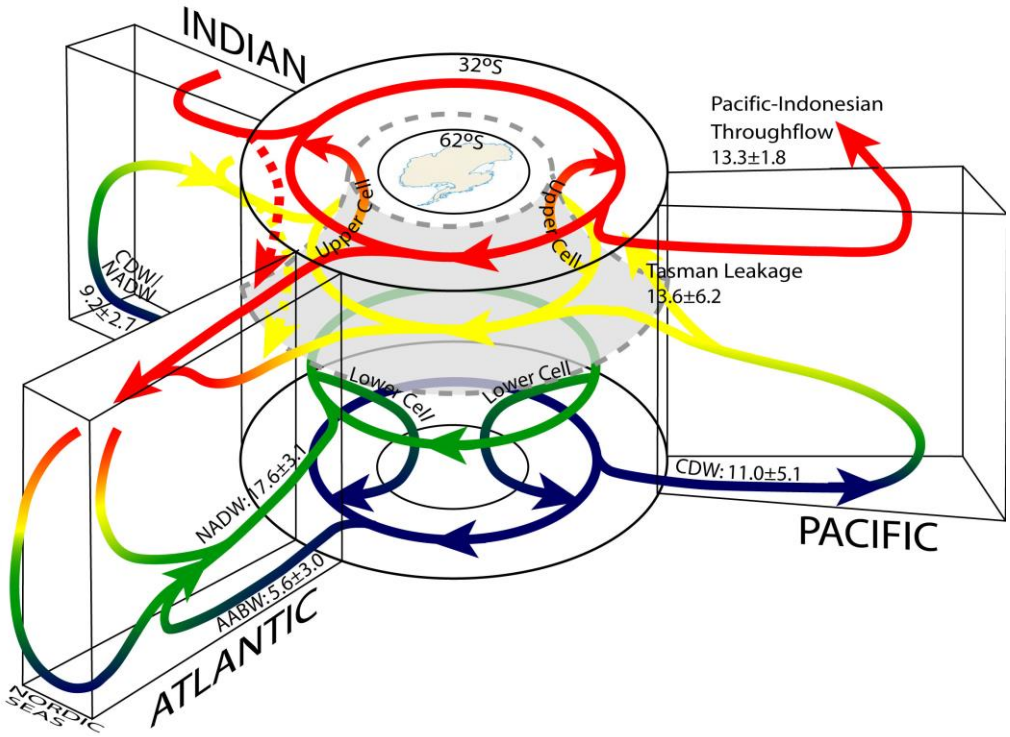

Figure 1 — A schematic of the global Meridional Overturning Circulation, showing the key linking role of the Southern Ocean (Lumpkin and Speer, 2006). Labelled water masses: North Atlantic Deep Water [NADW], Circumpolar Deep Water [CDW] and Antarctic Bottom Water [AABW], with associated Sverdrup transport.

1.2 - LARGE SCALE CIRCULATION AND BATHYMETRY OF THE SOUTHERN OCEAN

Dominating the circulation of this region is the strong, deep-reaching, eastward-flowing Antarctic Circumpolar Current [ACC], which runs unbroken around the globe and is roughly 25 000 km in length (Rintoul and Naveira Garabato, 2013). The ACC was once known as the 'West Wind Drift' and is predominantly driven by the strong westerly winds which prevail between 30-65˚S (Trenberth, Large, & Olson, 1990). The presence of the ACC could be used to define the northern limit of the SO, at approximately 38°S, which is the northernmost excursion of the ACC (Talley, 2011). Two cyclonic 'subpolar' gyres lie south of the ACC, one in the Weddell Sea and the other in the Ross Sea, as seen in Figure 2. As a consequence of these gyres there is a westward flow along the Antarctic coast. Close to the Antarctic continent the winds are easterlies; these can be very strong as a result of continental forcing from the northward katabatic winds which come from the Antarctic landmass (Talley, 2011). These easterlies drive Ekman transport towards the continent, inducing downwelling at the continental boundary.

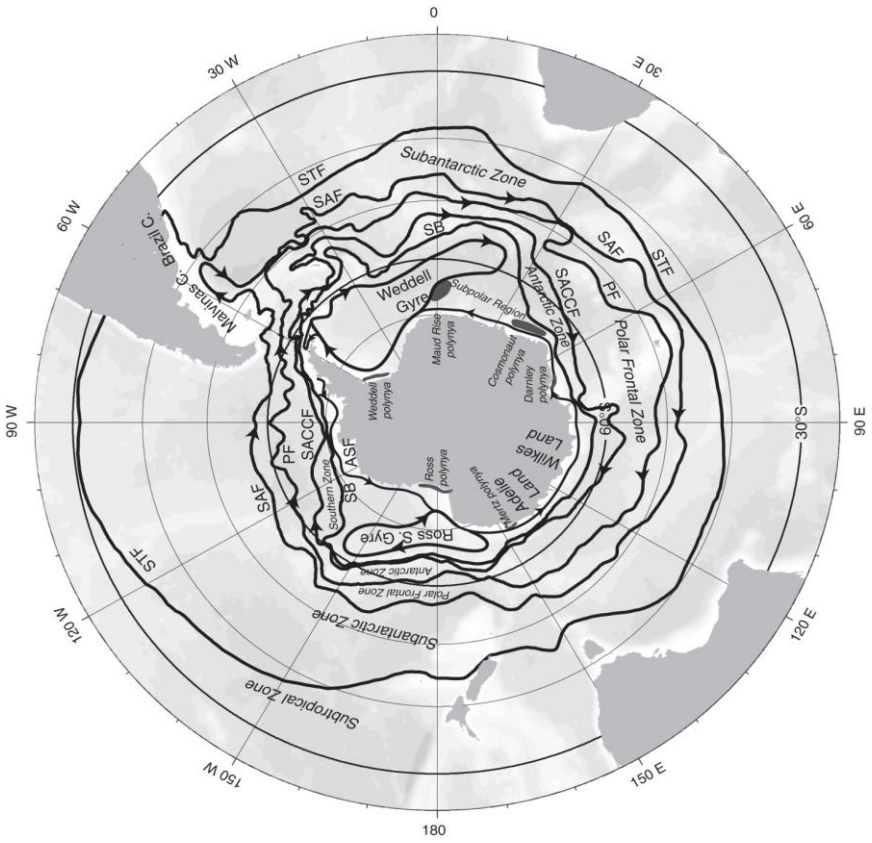

Figure 2 – A schematic depicting the mean positions of the principle fronts of the Southern Ocean: Subtropical Front [STF], Subantarctic Front [SAF], Antarctic Polar Front [APF], Southern ACC Front [SACCF], Southern Boundary [SB] and Antarctic Slope Front [ASF] [arrows show the jet flow direction]. The main polynyas are shown by dark grey patches and appropriately labelled as such. Oceanic zones are also represented. Image created by Talley (2011), with front locations from Orsi et al. (1995).

The bathymetry of the Southern Ocean is comprised of deep [>4000 m] ocean basins interspersed with numerous shallow mid ocean ridges and prominent plateaus, the depths of which range between 500 – 2000 m [Figure 3]. While the zonal continuity of the ACC is a most striking feature, the path and width of the ACC varies significantly. This variation in the ACC is as a result of the current being severely obstructed by various topographic features within the southern ocean (Talley, 2011). Therefore, the ACC has been shown from numerous studies (Orsi et al., 1995; Lenn et al., 2007) to meander during its circumpolar passage [Figure 2]. The ACC curves furthest north just off the coast of Argentina in the southwest Atlantic [northern edge at 38°S], and extends the furthest south upstream of the Drake Passage in the southeast Pacific [northern edge at 58°S]. These meander limits are shown in Figure 2. Mid-ocean ridges of the Southern Ocean also result in strong steering of the ACC through gaps in the ridges. A lesser known topographic feature affecting the flow of the ACC is the South West Indian Ridge [SWIR], which lies between Africa and Antarctica (Pollard and Read, 2001; Ansorge and Lutjeharms, 2003). Park et al. (2001) approximated that, south of Africa, the ACC transports 160Sv while in a similar study (Sloyan and Rintoul, 2001) 135Sv has been estimated, highlighting the variability associated with the ACC in this sector of the SO. These variations of current transport in these two papers are also likely to be a result of differing methodologies. For instance, Park et al., (2001), did not include direct current measurements in their study.

Closer inspection of the structure of the eastward flowing ACC (Pollard and Read, 2001; Sokolov and Rintoul, 2009) has made it clear that the frontal structure of the ACC is comprised of many fragmented branches, as also described by Talley (2011) and depicted in Figure 2.

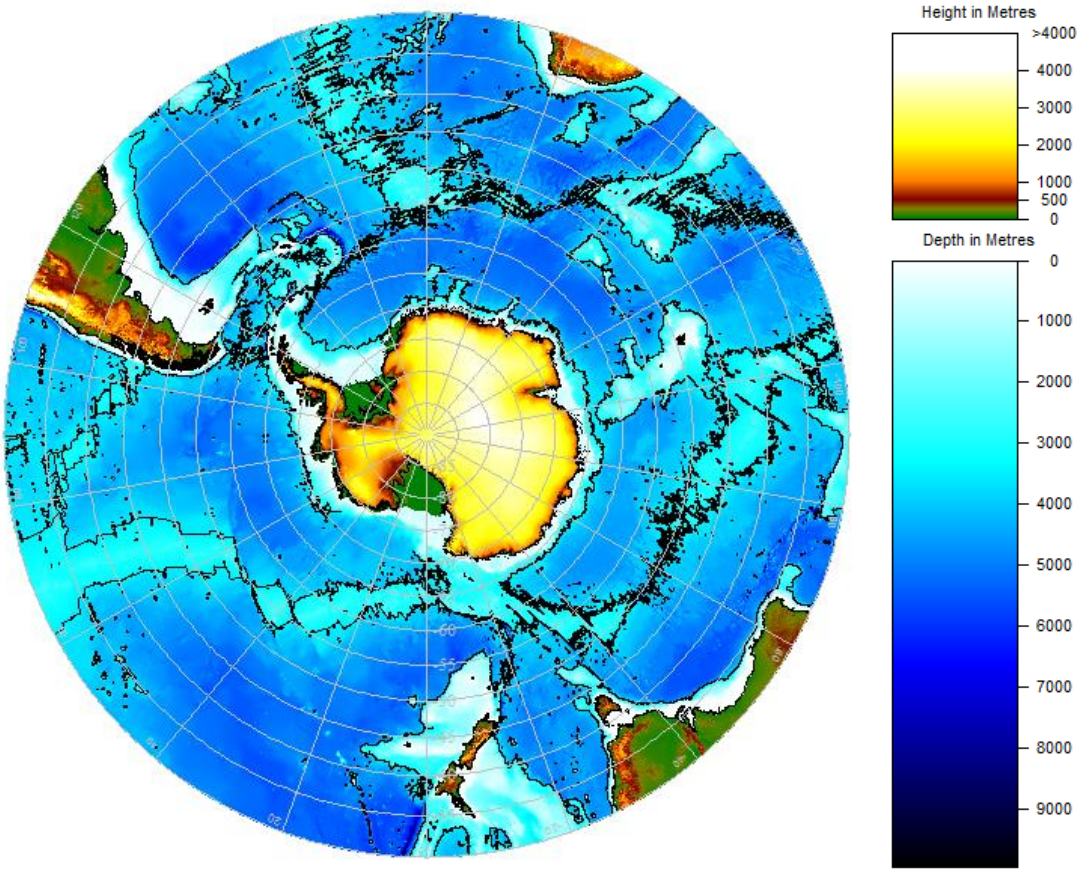

Figure 3 – Bathymetry of the Southern Hemisphere with the bathymetry [depth] and land topography [height] scales to the right. The coastal and the 3500m contours are shown by black contour lines. Image created with GEBCO.

1.3 - FRONTAL DEFINITION OF THE ANTARCTIC CIRCUMPOLAR CURRENT

Previous studies (Sokolov and Rintoul, 2007; Talley, 2011) have shown that the ACC is not a uniform eastward flowing current, but consists of multiple quasi-permanent jets [Figure 2], both at the surface and at depth, which are known to separate the ACC into different zones of distinct water masses. These multiple jets or fronts, characteristic of the ACC, have been observed in a number of datasets including; sea surface temperature data (Hughes and Ash, 2001), dynamic height fields derived from surface drifters (Niiler et al., 2003; Hughes, 2005), repeat hydrographic sections (Sokolov and Rintoul, 2007), sea surface height measurements (Sokolov and Rintoul, 2007, 2009) and repeat acoustic Doppler current profiler [ADCP] transects (Firing et al., 2011). The flow within the fronts is eastward and strong; the highest speeds are found in the Subantarctic Front [SAF] [30 to 70 cm/sec] and the Antarctic Polar Front [APF], which is nearly as energetic [30 to 50 cm/sec] (Hofmann, 1985). However, in the zones between the fronts, the flow is dominated by the presence of eddies whose characteristic rotation results in the flow being multidirectional (Talley, 2011). The positions of these jets are typically defined as narrow regions where there is a measurable hydrographic transition accompanied by a strong geostrophic flow. More specifically, there is either the presence of a particular water property mass at a particular depth or there is

a change between water property combinations typical of the zones between the fronts. An example of this in the Southern Ocean is the change from light subtropical water in the north, to cold, dense, Antarctic water in the south (Sokolov and Rintoul, 2002).

These fronts and zones are those which are present within the region around the Andrew Bain Fracture Zone [ABFZ] of the South West Indian Ridge [the research area of this thesis]. The relevant fronts, as described by Talley (2011), are; the Subantarctic Front [SAF], the Antarctic Polar Front [APF] and the Southern ACC Front [SACCF]. The Southern Boundary [SB], found south of the SACCF. The zones related to these fronts are; the Antarctic Polar Frontal Zone [APFZ; between the SAF and the APF], the Antarctic Zone [AAZ; between the APF and SACCF], the Southern Zone [SZ; between the SACCF and SB] and the Subpolar Zone [SPZ; south of the SB] (Orsi et al., 1995). The fronts and zones listed above are depicted in Figure 2 above. It is now known that the SO is an area of high variability, made up of a complex network or eddies and jets shown in Figure 4.

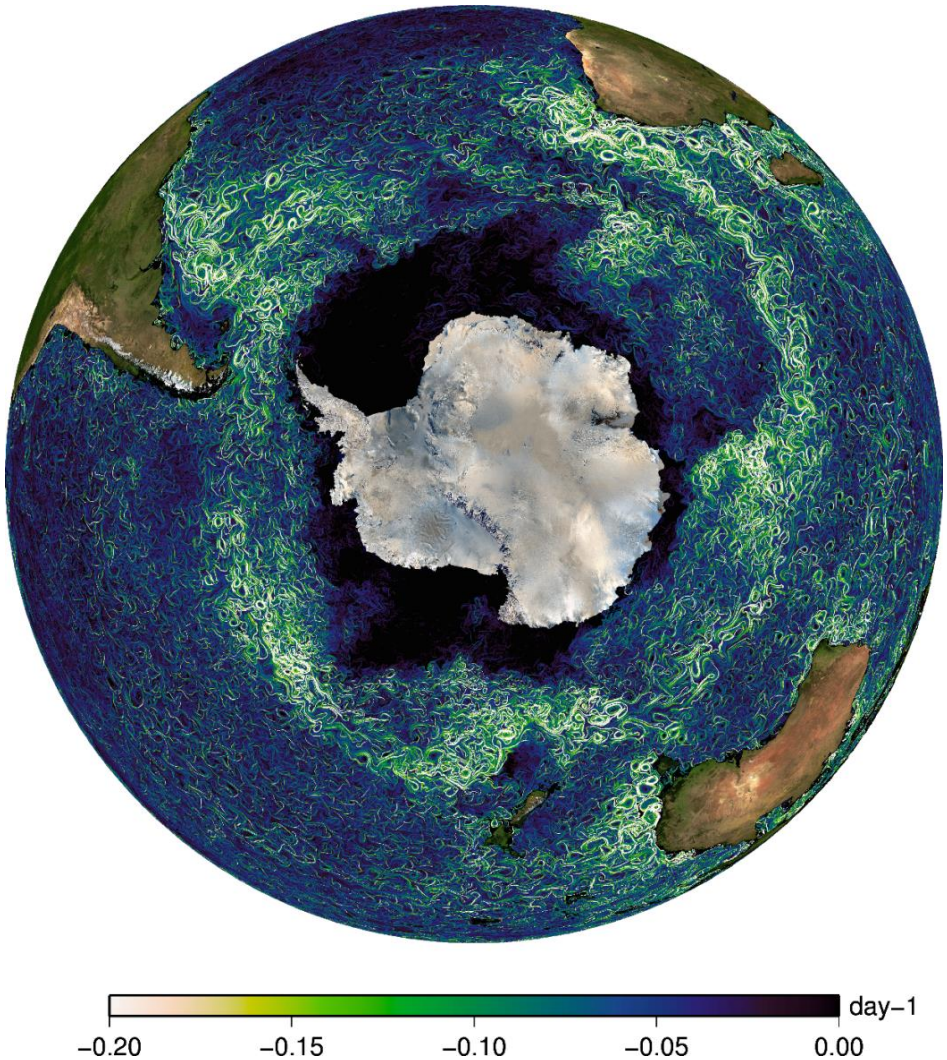

Figure 4 – The mesoscale ocean circulation [lyapunov exponents] around Antarctica for 27 May, 2014. From the image scale at the bottom of the image; white to green trajectories represent relatively high mesoscale velocities and blue areas show regions of relatively weak mesoscale velocities. Image distributed by *Aviso*, with support by *Cnes* and available from the website: http://aviso.altimetry.fr/.

1.4 - VARIABILITY ASSOCIATED WITH THE ANTARCTIC CIRCUMPOLAR CURRENT

While the track of the fronts may be circumpolar, they also display a strong temporal variability in latitude and structure (Talley, 2011) with large areas of substantial mesoscale activity dominating the core of the ACC [Figure 4 and 5]. Gille (2002) explained that highly detailed studies of these regions were relatively limited. However, since 2002, with the technological advancement of ocean sampling equipment, a new generation of observing systems have recently been put into practice. These new methods facilitate the improvement of our knowledge particularly in areas of weak coverage. These modern techniques include; remote sensing via satellite altimetry, in situ measurements with use of Argo floats, sensors attached to marine mammals and autonomously driven SeaGliders. Hydrological observations are important as they aid the description and understanding of the mesoscale processes which occur in and around the ACC within the SO (Budillon and Rintoul, 2003). These mesoscale processes take the form of; mesoscale eddies, frontal meanders, frontal splitting/merging and mesoscale divergence, all of which are typically found in areas of amplified mesoscale variability (Ansorge et al., 2006).

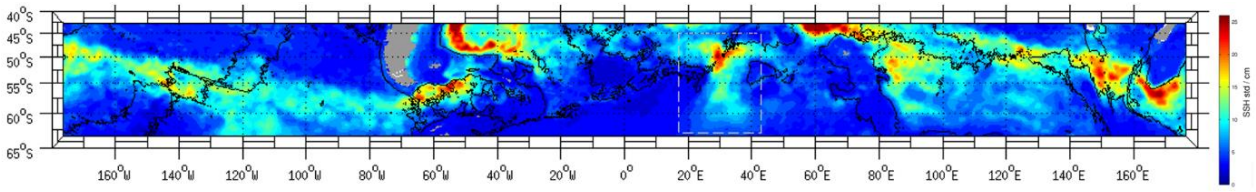

Figure 5 – The temporal sea surface height standard deviation, from satellite altimetry data for the period 1993-2009. The area of high mesoscale activity, south of the South West Indian Ridge, is shown enclosed by a dashed white line. Red to yellow areas signify areas of high sea surface variability, while cyan to blue areas signify regions of low sea surface variability. Basic bathymetry is shown by the 3500m isobath [black line]. Image provided courtesy of Sam Ebernez, GEOMAR, Helmholtz Centre for Ocean Research.

Note: Due to page size restrictions a larger version of Figure 5 is placed in the appendix: Appendix A. A zoomed in version of the area demarcated by the dashed white box is featured later in this thesis: Figure 7.

Archival results from numerous sources, such as measurements ranging from early ship's data (Gordon et al., 1978; Lutjeharms and Baker, 1980), surface drifters (Hofmann, 1985), satellite altimetry (Sandwell and Zhang, 1989) and numerical model studies (Gille, 1997) show that mesoscale variability within ocean currents is dependent on the topography over which that current is flowing. The stretching or squeezing of a moving water column has an influence on the vorticity of that water (Moore et al., 1999), so that where topographic constraint is low [i.e. within deep ocean basins], mesoscale variability in the overflowing water is limited. Conversely, in zones of topographic complexity [i.e. ocean areas occupied by seamounts, passages or chokepoints, continental shelves, islands, fracture zones and/or ridges], the mesoscale variability contained in the overflowing current is enlarged. The phenomena which are created due to mesoscale variability include; current meanders, divergence/convergence of the fronts of currents and the formation of mesoscale eddies. The track of the ACC is jointly directed by wind and buoyancy/density forcing (Hogg, 2010) as well as by the topography of the ocean floor over which it flows. Examples of topographic features which induce mesoscale variability into the ACC, and so guide its course, are; the continental shelf South of New Zealand (Bryden and Heath, 1985), the South West Indian Ridge [SWIR] (Ansorge and Lutjeharms, 2003; 2005), the Drake Passage (Lenn et al., 2007), the Conrad Rise (Durgadoo et

al., 2008) and the Kerguelan Plateau (Roquet et al., 2009). The mesoscale activity created by these features is shown in Figure 5. Of these bathymetric features, it is the South West Indian Ridge and its influence on the mesoscale activity [specifically the mesoscale eddies] of the ACC which is of prime importance to this thesis.

1.5 - THE SOUTH WEST INDIAN RIDGE AND RELATED MESOSCALE EDDIES

The South West Indian Ridge, which is the tectonic spreading margin between Africa and Antarctica, extends northwards towards southern Madagascar and is broken into a series of fracture zones (Sclater et al., 2005). The Du Toit, the Andrew Bain [ABFZ, Figure 6] and the Marion and Prince Edward fracture zones cross cut this ridge between 25°E and 35°E. Hydrographic data collected during the SWINDEX [South West Indian Ocean Experiment] surveys in 1993 and 1995 have shown that, on encountering this ridge, the ACC splits into several branches (Pollard and Read, 2001) which results in enhanced mesoscale eddy generation extending downstream of this region (Ansorge and Lutjeharms, 2003; Ansorge et al., 2006). Later, between 2003 and 2005, the Dynamics of Eddy Impacts on Marion's Ecosystem [DEIMEC] surveys were conducted in this area of the SWIR (Durgadoo et al., 2010). Durgadoo et al. (2010) also identified the meandering and converging of fronts associated with the SAF and APF, together with the shedding of mesoscale eddies from these meanders. Thus areas of high mesoscale variability [Figure 5], associated with topographic features, can be regarded as being mesoscale eddy hotspots.

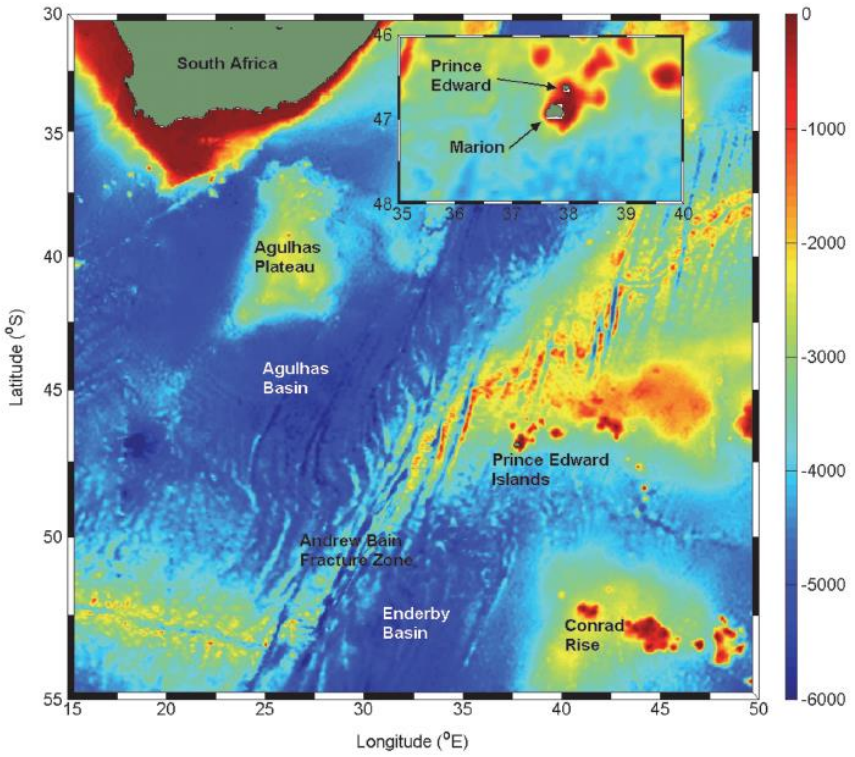

Figure 6 – Schematic depicting the bathymetry for the South West Indian Ocean from ETOPO2 data, with an insert of a zoom-in of the Prince Edward and Marion Island group and the surrounding bathymetry [isobaths are in metres]. (Durgadoo et al., 2010)

Durgadoo et al. (2011) and Ansorge and Lutjeharms (2003; 2005) described the region immediately downstream of the Andrew Bain Fracture Zone [ABFZ] section of the SWIR as an eastward propagating eddy corridor, bordered by the Del Cano Rise to the north and the Conrad Rise to the south [Figure 6].

Durgadoo et al. (2011) evaluated the properties of cyclonic mesoscale eddies found within this eastward propagating eddy corridor because, due to the upwelling of deep nutrient rich water, such cyclonic eddies are highly influential on the marine ecosystems of the Prince Edward Islands [PEI] (Durgadoo et al., 2010).

South of the eddy formation region of the ABFZ, a second prominent feature of sea surface height variability is present [extending south]. This feature, highlighted by a dashed white box in Figure 5, extends southwards in contrast to the above mentioned eastward extending eddy corridor. Unfortunately, minimal oceanographic research in this region has so far constrained our understanding of this southward extension and whether it is another corridor of mesoscale eddies, as sea surface anomaly [SSHA] plots appear to suggest.

While the influence that the South West Indian Ridge [SWIR] has on the mesoscale variability of the Antarctic Circumpolar Current [ACC] is well known, the area of high mesoscale variability within 20°E - 45°E, which extends from 45°S to ±60°S [marked by the dashed white box in Figure 5], has not been well investigated. Our understanding of the gradual southward dissipation of this area of high mesoscale activity, and the dynamics within it over a period of time, remains limited. Key questions with regards to this southward extending corridor of mesoscale activity are as follows:

1.6 - KEY QUESTIONS

1. Have there been any mesoscale eddies travelling southwards from the SWIR since 2012?
2. What are the trajectory characteristics of the southward propagating mesoscale eddies?
3. How are these mesoscale features structured hydrographically?

An in-depth analysis of these mesoscale features, including where and how they may advect southwards, their hydrographic structure, water mass characteristics and the heat fluxes associated with them, needed to be undertaken. By addressing the above key questions, the impact that southward migrating anticyclonic eddies may have on the surrounding waters, through their possible role in the exchange of heat and salt across the ACC and how they impact on global climatic and oceanic signals, will become clearer. The resultant implications, with regards to such a southward chain of eddies, are therefore of high importance in the acquisition of a better understanding of the role that the advection of such mesoscale eddies [across the ACC] play in global climate change.

2 - INTRODUCTION

2.1 - THE SOUTH WEST INDIAN RIDGE

The South West Indian Ridge [SWIR] has been shown to be a breeding ground for mesoscale eddies (Ansorge and Lutjeharms, 2003; 2005) and forms a notable eddy hotspot [in the region ranging from 15 – 25 SSH std/cm] in altimetry images [Figure 5]. While the influence that the SWIR has on the Antarctic Circumpolar Current [ACC] mesoscale variability is well investigated, our understanding of the gradual dissipation of these eddies, and their pathways and life span, remains limited. Ansorge et al., (2015) focused their attention on an area of anomalous sea surface height [SSH] south of this eddy field within 20°E - 45°E and extending from 45°S to ±60°S [Figures 5 and 7]. In order to investigate this area of high sea surface height variability, Ansorge et al. (2015) used a dataset created by Chelton et al. (2011), along with an array of both ship-based and Argo in situ datasets, to show evidence confirming the presence of a southward extending mesoscale anticyclonic eddy corridor.

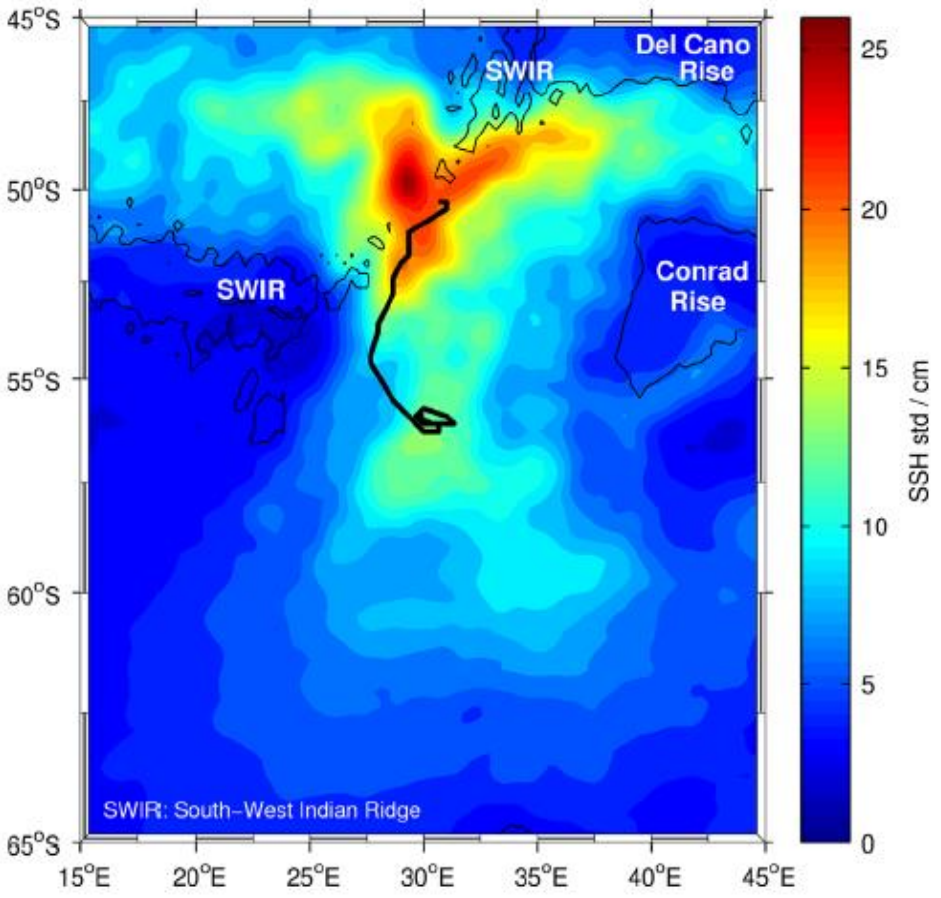

Figure 7 – Sea surface height standard deviation [scale to the right of image], from satellite altimetry data for the period 2000-2009. The bathometric features are shown by the 3500m black isobaths lines and are labelled accordingly; South West Indian Ridge, Del Cano Rise and the Conrad Rise. The trajectory of an anticyclonic eddy is depicted by a thick black line. (Ansorge et al., 2015)

2.2 - RESEARCH IN THE REGION SOUTH OF THE SOUTH WEST INDIAN RIDGE

While the frontal character and eddy activity of the eastward extension of the area of high mesoscale activity is well known (Durgadoo et al., 2011), the zone of diminishing mesoscale variability which extends southwards to approximately 60°S, has been poorly sampled. Past investigations of this area and its associated eddy field has been previously published (Gouretski and Danilov, 1993; 1994, Schröder and Fahrbach, 1999), but given the recent technological advances in both remotely-sensed observations and through the Argo array, a revision of this study could be justified. In their study, Gouretski and Danilov (1994) found that five anticyclonic eddies relocated southwards during the period of November 1986 and October 1988, propagating at a rate of 3cm.s^{-1}, until they dissipated between 55°S and 57°S. Gouretski and Danilov (1994) analysed these eddies hydrographically, however the results, as previously mentioned, are dated. With the recent development of ocean sampling methods using more technologically advanced equipment [such as; remote sensing via Argo floats, SeaGliders and satellite altimetry] we obtain a more updated understanding of the dynamics within the SO. Thus, a recent article, Ansorge et al. (2015), revisited this region, with more contemporary technology, and so refocused the oceanographic community's attention on the possible role this southward extending area of mesoscale variability would have on the surrounding ocean environment. In doing so, the existence of the southward extending anticyclonic mesoscale eddy corridor was confirmed by Ansorge et al. (2015).

2.3 - RECENT EVIDENCE OF A SOUTHWARD EXTENDING ANTICYCLONIC EDDY CORRIDOR

The region of high sea surface height variability, shown in Figures 5 and 7, extends south from the Andrew Bain Fracture Zone [ABFZ] section of the SWIR. From satellite altimetry data for the period 2000-2009, Ansorge et al. (2015) plotted the sea surface height standard deviation of this region and demarcated the trajectory of a single anticyclonic eddy using a thick black line [Figure 7]. Studying the plotted trajectory of the anticyclonic eddy, it is seen that the southward advection falls within the region of high sea surface height variability. Creating a Map of delayed time Absolute Dynamic Topography [MADT], merged with sea level anomaly data, produced the mean frontal positions of the ACC shown in Figure 8. This figure shows the routes which the ACC fronts take as a result of the SWIR influence on their potential vorticity. When compared to the other fronts of the ACC, the path of the southern boundary front [SACCF], shown in blue, deviates the furthest south, which reaffirms the SWIR's influence on the ACC. Ansorge et al. (2015) also found that 28 eddies were propagating south [25 anticyclonic and 3 cyclonic] during a 19 year period, at a rate of 1.4 eddies per year. The trajectories of these eddies, shown in Figure 9, run parallel to the track of the SACCF and also fall within the region of high sea surface height variability. The examination of the manner by which these 25 anticyclonic eddies propagated south, and their scalar changes, was not the focus of Ansorge et al. (2015). However, this thesis ventures to investigate and compare the individual

characteristics of the mesoscale features which have been found to propagate south through the eddy corridor.

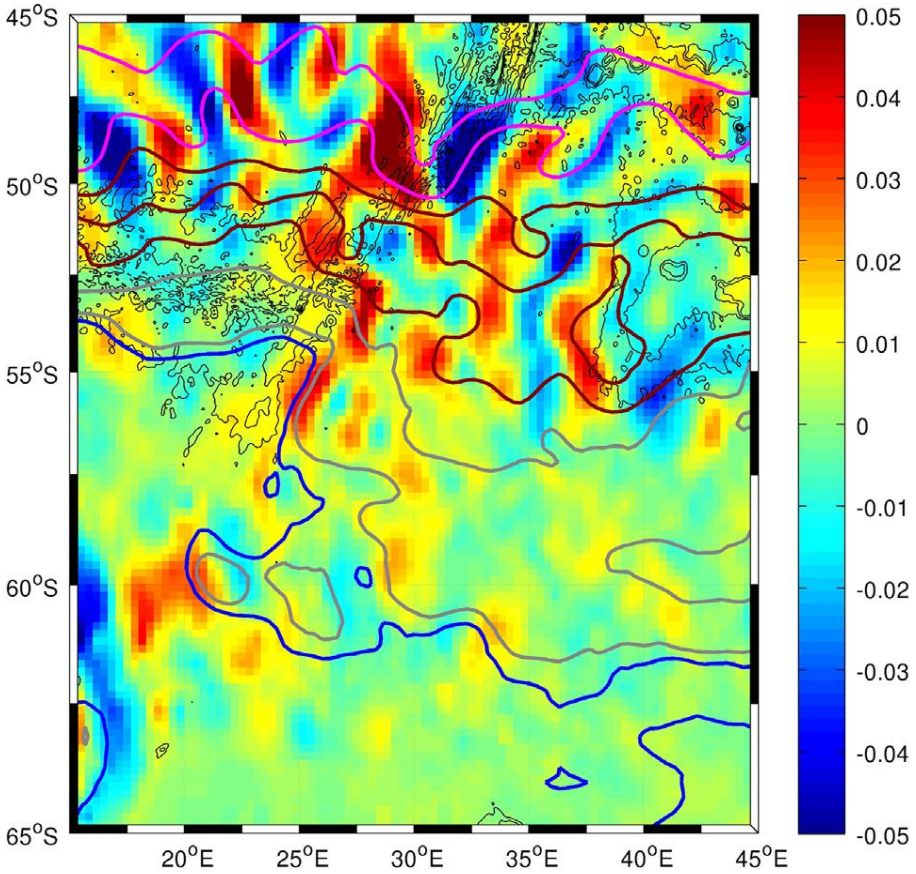

Figure 8 – A delayed time Map of Absolute Dynamic Topography [MADT] of a section of, and south of, the South West Indian Ridge, between January 2006 and December 2007. The MADT scale is on the right of the image: units used 'dyn m/25km'; the MADT values are related with the anomaly field. The mean location of fronts of the Antarctic Circumpolar Current [ACC] are overlaid; the northern, middle and southern branches of the Sub-Antarctic Front [pink], Antarctic Polar Front [magenta], Southern ACC Front [grey] and the Southern Boundary of the ACC [blue]. The simplified bathymetry of the region is shown with black contours [isobaths from 500m to 3500m with 1000m intervals]. (Ansorge et al., 2015)

Due to this southward passage of anticyclonic mesoscale eddies, heat, salt and biota, entrapped by these eddies, are subsequently transported across the ACC and further south within the SO. The potential of this phenomenon to influence the dynamics and characteristics of the SO is of prime importance, therefore dedicated ship time was approved in 2013 to hydrographically sample mesoscale eddies, within this southward extending eddy corridor, in order to improve our understanding of the role the eddies play. This dedicated ship time was undertaken in April/May 2014 during the 2014 Marion Island Relief Cruise [MIRC2014].

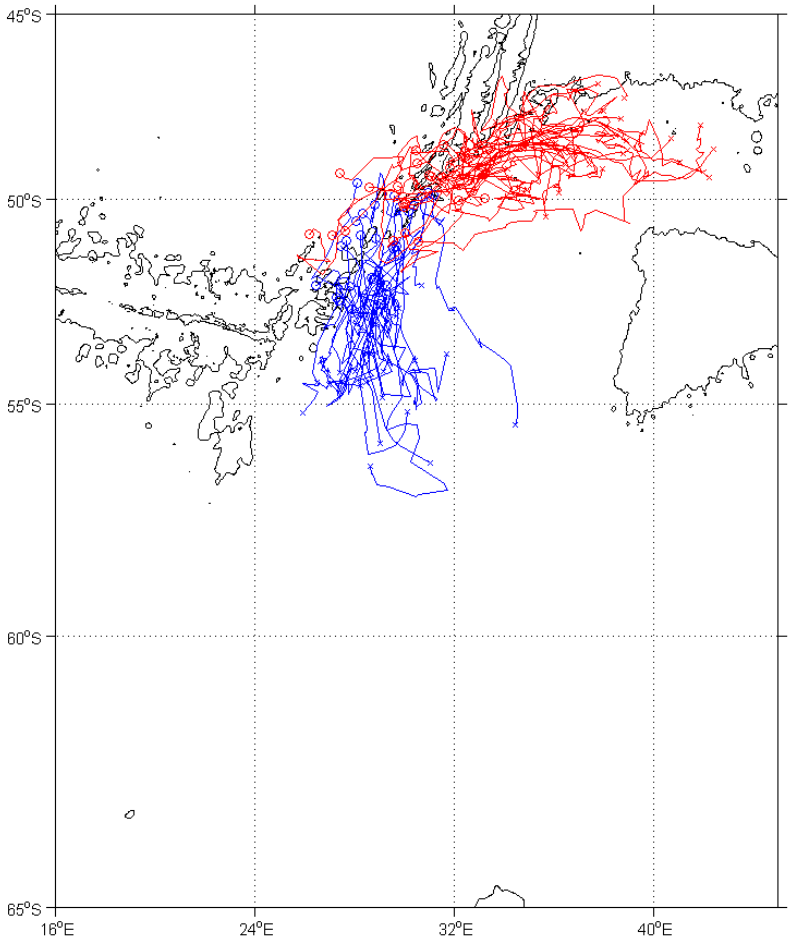

Figure 9 – Sea surface height [SSH] anomalies tracked using the Chelton et al. (2011) eddy tracking algorithm for the period 1992 – 2012. Blue lines represent the trajectories of 25 positive anomalies which propagated southwards, while red lines represent the 28 positive and negative anomalies that moved eastward in to the area of the Prince Edward Islands. Each trajectory is comprised of a starting position [symbolized by an o], the eddy's path [shown by a line] and the track termination [demarcated by an x]. The 3500m isobath was used to depict the basic bathymetry of the region. (Ansorge et al., 2015)

2.4 - THE INTENTION OF THIS STUDY

This study investigates anticyclonic mesoscale eddies, identified within the southward extending anticyclonic eddy corridor, by focusing on their behaviour and structure through a combination of both satellite altimetry and in situ measurements. This thesis builds on the article by Ansorge et al., (2015), by providing more detailed oceanographic characteristics of the anticyclonic eddies identified within this southward corridor. Using the in situ hydrographic data collected during the MIRC2014, on board the SA Agulhas II, two anticyclonic eddies within the southward eddy corridor were studied using data from both CTD and XBT deployments.

There are three objectives to this thesis, which encompass the key questions set out in the previous section. The first objective is to more comprehensively understand the eddy characteristics within the confirmed southward anticyclonic eddy corridor, by creating a series of Hovmöller plots using recent delayed time satellite altimetry data. The second objective analyses the 25 historical eddy trajectories found by Ansorge et al. (2015) in order to determine their trajectory characteristics and scalar changes. The third objective is to compare, hydrographically, two particular anticyclonic mesoscale eddies found and sampled within the southward eddy corridor.

3 - DATA and METHODS

3.1 - ARE THERE MESOSCALE EDDIES TRAVELLING SOUTHWARDS FROM THE SWIR?

Within the region of the Southern Ocean south of Africa, the South West Indian Ridge [SWIR] acts as a breeding ground for mesoscale eddies (Ansorge and Lutjeharms 2003; 2005). While the influence that the SWIR has on the Antarctic Circumpolar Current [ACC] mesoscale variability is well investigated, the knowledge of the dynamics of these mesoscale eddies, specifically those which are propagating south of the SWIR, remains limited.

The intention of this first objective is to understand the eddy trajectory characteristics within this southward extending anticyclonic mesoscale eddy corridor. This objective uses delayed time Sea Surface Height Anomaly [SSHA] data for the time period 1 May 2012 to 31 May 2014. The survey performed by Ansorge et al. (2015) confirmed that this area is a corridor of mesoscale eddies. Therefore it can be surmised that the anomalies found in the research area, by means of the following Hovmöller analysis, are mesoscale eddies. In order to determine the contemporary eddy trajectory characteristics, the following data and methods were used.

3.1.1 - SURFACE HEIGHT ANOMALY DATA

To determine recent eddy dynamics within the southward extending eddy corridor, a series of 7 Sea Delayed Time Surface Height Anomaly [SSHA] latitude-time Hovmöller plots were created using the Aviso website (http://las.aviso.oceanobs.com/las/getUI.do). The Hovmöller analysis scheme allowed for the mesoscale eddy propagation tracks to be confidently and continuously investigated as time passed. The Aviso data set was chosen due to its homogeneous catalogue of products, which is as a result of merging multiple satellite data products. This merging also provides a data set with a high resolution, which is necessary for mesoscale features to be studied. The plots created using the Aviso website extend from 48° - 57°S, with the same scale [-0.5m – 0.06m] with a contour interval of 0.05m. The Hovmöller plots corresponding to these lines are described and discussed in the Results and Discussion section [Section 4.1]. It is notable that the Hovmöller lines in the western half of the eddy corridor are close together, as there was a higher population of eddy tracks in this area (Ansorge et al., 2015). On the eastern side of the eddy corridor, where there was an area of far lower variability noted by Ansorge et al. (2015), the Hovmöller lines are spread further apart, see Table 1.

3.1.1.1 - LONGITUDE EXTENT

SSHA data for these lines date from May 1st 2012 to May 31st 2014 and consequently include the eddies sampled during the 2014 Marion Island Relief Cruise [MIRC2014]. The latitudes of each Hovmöller plot, together with its corresponding figure number, are as follows:

Table 1 – The 7 Hovmoller transects, their corresponding longitude of each Hovmöller plot, together with their matching figure number.

TRANSECT NUMBER	LONGITUDE	FIGURE NUMBER
1	25.4°E	15
2	27.4°E	16
3	28.4°E	17
4	29.4°E	18
5	31.4°E	19
6	34.4°E	20
7	39.9°E	21

These Hovmöller lines cover sections west, east and within the eddy corridor. Figure 10 shows the array of Hovmöller lines, using the 3500m ETOPO2v2c isobath for a bathymetric indicator of the South West Indian Ridge [SWIR].

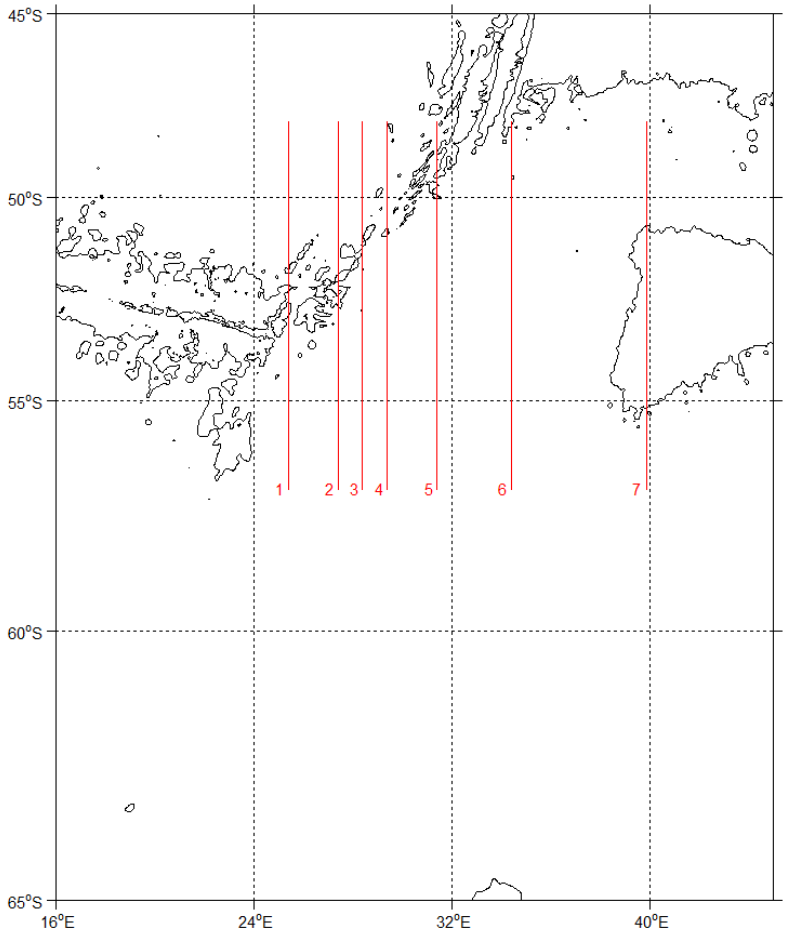

Figure 10 – Hovmöller transects which ran from 48° - 57°S are marked in red. From west to east [1 – 7] the Hovmöller latitudes were; 25.4°E, 27.4°E, 28.4°E, 29.4°E, 31.4°E, 34.4°E and 39.9°E. The 3500m isobath was used to depict the basic bathymetry of the region.

3.1.1.2 - LATITUDE EXTENT

The southward extent of the 7 Hovmöller lines used in this thesis were specifically selected because they constituted a spread right across the area of the southward extending anticyclonic eddy corridor and are expected to provide an a temporally uninterrupted depiction of the domain of this region of high variability, between 48° and 57°S. The following SSHA Hovmöller images show the mesoscale eddies relevant to this study and are described in Section 4.1. It should be noted that for each of the delayed time sea surface anomaly images [Figures 13 – 19], the right hand scales of the SSHA are the same.

3.1.2 - BATHYMETRY

An appropriate, comprehensive and commonly used bathymetry data set was required for use in this thesis. The bathymetry dataset, ETOPO2v2c, is a cell-centred dataset and has a resolution of 0.15°x0.3° or 2-minute horizontal resolution. This ETOPO2v2 Global Relief Model was built from numerous global and regional datasets that integrated land topography and ocean bathymetry. This ETOPO2v2c data set was downloaded from the NOAA website: http://www.ngdc.noaa.gov/mgg/fliers/06mgg01.html, and was used throughout of this thesis.

3.2 - WHAT ARE THE TRAJECTORY CHARACTERISTICS OF THE SOUTHWARD PROPAGATING MESOSCALE EDDIES?

Within the region of high mesoscale activity associated with the South West Indian Ridge [SWIR], Ansorge et al. (2015) focused their attention on an area of anomalous sea surface height [SSH] within 20°E - 45°E and extending from 45°S to ±60°S [Figures 5 and 7]. In order to further investigate this area of high sea surface height variability and the southward propagation of individual mesoscale eddies, Ansorge et al. (2015) used a previously compiled global dataset created by Chelton et al. (2011). To compile this dataset, Chelton et al. (2011) conducted a global survey of the characteristics and behaviour of the mesoscale eddies of the world's oceans. The resulting dataset describes the distribution and the trajectories of global mesoscale eddies [along with scalar variables] for the period October 1992 – April 2012. This data set is particularly comprehensive, due to the inclusion of multiple scalar properties and its temporal length in regard to mesoscale features. For consistency with the Ansorge et al. (2015) survey, the Chelton data set was used in this thesis' survey.

The objective investigates historical eddy track characteristics within the southward extending anticyclonic eddy corridor by using the trajectories of the 25 southward propagating anticyclonic eddies investigated by Ansorge et al. (2015). The previously compiled dataset by Chelton et al. (2011), describing the distribution and tracks [along with the scalar variables: sea surface height extremum, circum-average speed and radius] of global mesoscale eddies which was used by Ansorge et al. (2015), was paired with ETOPO2v2c ocean bathymetry [previously mentioned in Section 3.1 above]. This pairing was implemented in order to investigate the historical mesoscale eddy track characteristics and scalar changes in the area south of the Andrew Bain Fracture Zone [ABFZ] section of the SWIR, between October 1992 and April 2012.

3.2.1 - THE CHELTON et al. (2011) DATASET:

The Chelton et al. (2011) dataset used satellite altimetry, which identified sea surface height [SSH] contours, and used an automated tracking scheme in order to detect mesoscale eddies and to determine their trajectories. The SSH data used to track eddies was derived from the satellite altimeters TOPEX/Poseidon and ERS-1/2, with a resolution of 0.25° x 0.25°. This dataset tracked eddies from October 14, 1992 to April 4, 2012 [19.5 years] and consists of 215184 globally tracked eddies, with a 7 day time step between each observation. Once an eddy was identified, it was tracked from one time step to the next by locating its characteristic eddy centre (Chelton et al., 2011). The researchers acknowledged that complications and misidentified eddies are possible in areas of energetic mesoscale activity, where merging, splitting and/or distortion is common. To avoid this, Chelton et al. (2011) focused on features with lifetimes greater than 16 weeks in their analysis. Furthermore, features in the area which are smaller than the area Rossby radius of deformation [<10km] will not have been detected successfully by the tracking scheme.

The eddy properties determined by Chelton et al. (2011), include; latitude, longitude, eddy identification number, observation sequence number [sampling interval], Julian date, polarity [cyclonic being -1 and anticyclonic being +1], amplitude, radius and maximum circum-averaged speed. The details of the scalar variables; radius, maximum circum-averaged speed and amplitude, are as follows:

- The eddy radius is defined as the radius of a circle whose area is equal to that enclosed by the contour of maximum circum-average speed. The radius range was 9.42582 - 444.155 km.
- Maximum circum-averaged speed is defined as the average speed of the contour defining the radius scale L. The maximum circum-averaged speed range was 0.58823 -563.817 cm/sec.
- Amplitude is defined as the magnitude of the height difference between the extremum of SSH within the eddy and the SSH around the contour defining the eddy perimeter. The amplitude range was 1.00001 - 125.935 cm.

A subset of 25 eddies, isolated by Ansorge et al. (2015), from the global eddies of Chelton et al. (2011), were the subjects of this section's investigation. The criteria used in this thesis to select the 25 southward propagating anticyclonic eddies to be studied, were the same as that implemented by Ansorge et al. (2015). These criteria excluded eddies with incorrect origin positions [not proximal to the ABFZ section of the SWIR] and eddies with pathways which were not relevant to the survey were excluded from the survey [outside of the corridor region]. Of these, the tracks of five particularly pertinent eddies, that had relocated southwards along the eddy corridor, together with their scalar variation analysis, are included in the results [Section 4.2]. The eddy track plots of the remaining 20 eddies used by Ansorge et al. (2015), which are not pertinent to this section's results, are located in Appendix B. A table of the relevant eddy identity numbers, together with the total sampling interval of all 25 eddies used in this thesis can be found in Appendix C.

3.3 - HOW ARE THESE MESOSCALE FEATURES STRUCTURED HYDROGRAPHICALLY?

Past investigations have focused solely on remotely sensed information to track eddy activity in this region of high mesoscale activity south of the South West Indian Ridge [SWIR]. The physical properties of the features remained poorly understood until April 2014 when a dedicated voyage along the southern extension of this region was undertaken. This voyage took place in April/May 2014 during the MIRC2014 aboard the SA Agulhas II, with special focus on the oceanographic characteristics of anticyclonic eddies propagating south between the SWIR and the Conrad Rise and into the Enderby Basin [Figure 6].

This third objective comprises oceanographic testing of two particular anticyclonic eddies found to have propagated south from the SWIR, as noted in Objective 2 [Sections 3.2 and 4.2]. This objective uses; in situ data collected during the MIRC2014, real time Sea Surface Height Anomaly [SSHA] data, along with the ETOPO2v2c ocean bathymetry previously mentioned in Section 3.1. To complete Objective 3 the following data and methods were used:

3.3.1 - ALTIMETRY DATA

Real time Sea Surface Height Anomaly [SSHA] gridded data from the Aviso website (http://las.aviso.oceanobs.com/las/getUI.do) was used to depict the positions of the two anticyclonic mesoscale eddies sampled during the MIRC2014 [Figure 11]. These two eddies were transected between the 15th and 22nd of April 2014, so a median date of the 16th April 2014 was used in order to allow for the two eddies to be clearly visible in the same SSHA figure. In Figure 11, the positive anomaly centered over 30°E, 52°S [subsequently considered the 'juvenile' eddy], was sampled by Transect 1. The positive anomaly centered over 30°E, 57.5°S [subsequently considered the 'mature' eddy], was sampled during the second half of Transect 2 and all of Transect 3. The three transects of this objective are shown in Figure 12.

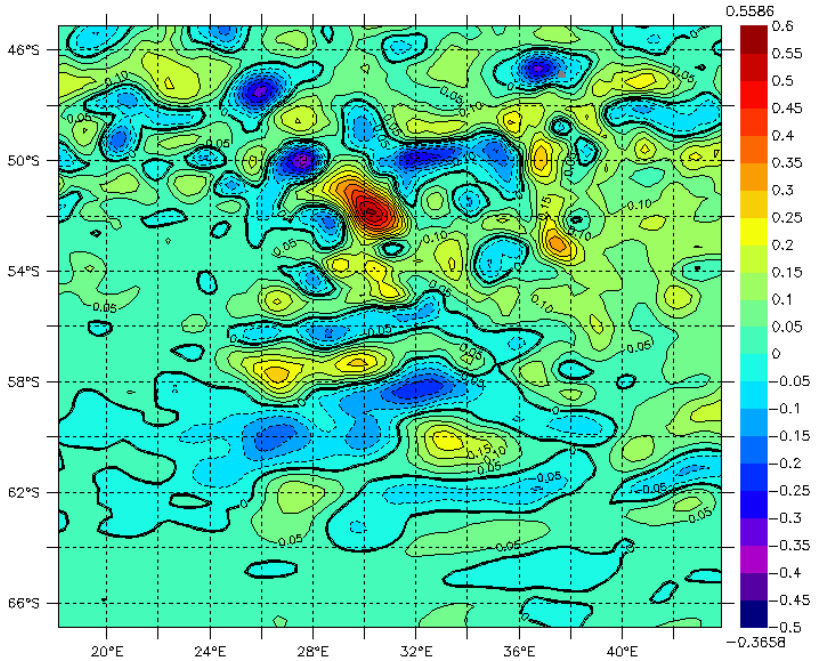

Figure 11 – A map of sea surface height anomaly [SSHA] over the region of interest from all available satellites on 16 April 2014. The SSHA scale is to the right in metres. Blue to purple areas represent negative anomaly values [cyclonic eddies] and yellow to red areas depict positive SSHA values [anticyclonic eddies]. The positive SSHA centered over 30°E, 52°S and the positive SSHA centered over 30°E, 57.5°S, are the two positive features sampled during the 2014 Marion Island Relief Cruise.

3.3.2 - 2014 MARION ISLAND RELIEF CRUISE OCEANOGRAPHIC DATA

In situ oceanographic data was collected as part of the survey of two particular anticyclonic mesoscale eddies in the region of the South West Indian Ridge [SWIR] during the 2014 Marion Island Relief Voyage. In total, 3 transects were completed; a zonal section of a juvenile anticyclonic eddy, a meridional section crossing both a cyclonic and mature anticyclonic eddy, and thirdly a zonal section transecting the mature anticyclonic eddy [previously transected by Transect 2]. During the MIRC2014 the instruments used to sample the ocean properties were; Conductivity, Temperature and Depth deployments [CTD] and Expendable Bathythermograph [XBT]. As mesoscale features are branded by their thermal properties and stratigraphic nature, the instruments used in this survey to define their vertical profiles are highly appropriate. The survey was conducted using full depth [between 3000m and 5000m] SBE 911plus CTD casts and 900m XBT underway deployments. The three transects over the Enderby Basin/SWIR region are depicted in Figure 12: transects are marked and labelled in grey, the CTD stations are represented by red dots and the XBT deployment positions are symbolized by blue dots. Unfortunately, due to extreme weather conditions, the number of stations planned for each eddy feature was substantially cut, with only a total of 15 CTD stations and 12 XBT deployments conducted during the eddy survey. The hydrographic variables relevant to this report, which were measured/calculated during the transects, were; temperature, salinity and depth [pressure]. Figure 12, created in Matlab, shows the bathymetry of the research area in relation to the transect positions and station type. The distance between each CTD/XBT station was, on average, 32.9 nautical miles.

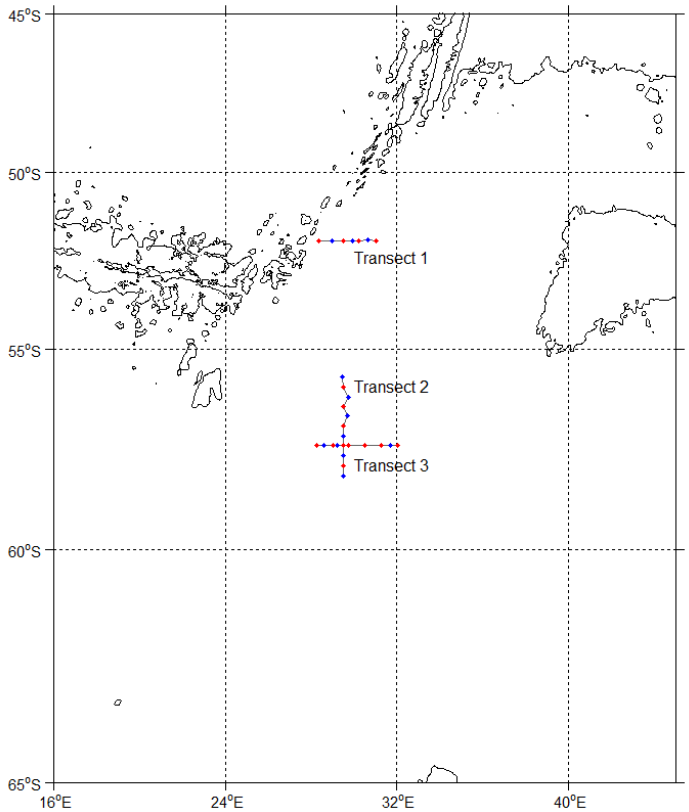

Figure 12 – Transects are marked and labelled in grey, the Conductivity, Temperature and Depth [CTD] stations are represented by red dots and the Expendable Bathythermograph [XBT] deployment positions are symbolized by blue dots. A total of 15 CTD stations and 12 XBT deployments were conducted during the 2014 Marion Island Relief Cruise survey. The 3500m isobath was used to depict the basic bathymetry of the region.

The data files from the CTD and XBT casts were converted in Seasave [Version 7], imported into Ocean Data View 4 and thus used to depict the hydrographic structure of the two mesoscale eddies. Temperature and salinity sections for each transect were created in order to visually portray each eddy's individual oceanographic characteristics. The temperature section of Transect 1 required a different temperature scale to that of Transect 2 and 3, as the 'juvenile' anticyclonic eddy was significantly warmer than the mature anticyclonic eddy. White isotherms, as opposed to the other black, are implemented in the three temperature sections, to be used as a reference for the transected eddies. Transect 1 [Figure 23] used the 2.6°C isotherm, while Transect 2 and 3 [Figure 26 and 28] used the 1.6°C. The use of the 2.6°C and 1.6°C isotherms are not used as scientific indicators. They are simply a way to define the shape of the features, relative to one another, within this thesis. More specifically, these isotherms have been used to depict where the majority of the mesoscale feature's individual temperatures are found. Temperature/salinity station plots for each transect were also created to allow for the water masses present within and around the two eddies to be identified. The images thus produced are in Section 4.3, Figures 25 – 30.

3.4 - CONFIDENCE OF METHODOLOGY

With the use of the high resolution of the Aviso dataset, combined with the temporal length and criteria associated with the Chelton et al. (2011) dataset, a detailed study of a mesoscale eddy corridor can be achieved with confidence. Further confidence is achieved by supplementing this dataset pairing with real-time stations, engaged during the MIRC2014. Despite there being a limited number of in situ stations executed during the voyage, the hydrographic data provided does present an important depth-view of the mesoscale features – which is not achieved by the previous two satellite-based datasets. Thus, a combination of these three datasets will provide a greater standing for this study's results.

4 - RESULTS and DISCUSSION

4.1 - ARE THERE MESOSCALE EDDIES TRAVELLING SOUTHWARDS FROM THE SWIR?

In order to understand the eddy characteristics within this southward extending anticyclonic mesoscale eddy corridor, this section analyses delayed time Sea Surface Height Anomaly [SSHA] Hovmöller plots for the time period May 2012 to May 2014. The data and methods described in Section 3.1 produced the following 7 Hovmöller plots of SSHA, for the 2 year period, and also a single day plot of SSHA, April 16th 2014. The 7 Hovmöller lines used in this thesis were specifically selected because they constituted a spread right across the area of the southward extending anticyclonic eddy corridor and should provide a temporally uninterrupted depiction of the domain of this region of high variability. The specific date of the 16th April 2014 was chosen as it was the median date to allow for 2 eddies, investigated by Objective 3, to be clearly visible in the same SSHA figure.

4.1.1 - SOUTHWARD EDDY CORRIDOR BOUNDARIES

Figure 13 [a side-by-side reel of the 7 Hovmöller transects] provides a depiction of how the domain of high Sea Surface Height [SSH] variability, in the region south of the South West Indian Ridge, fluctuated from May 2012 to May 2014. Blue to purple areas represent negative anomalies [cyclonic eddies] and yellow to red areas depict positive anomalies [anticyclonic eddies]. The SSHA scale is to the right in metres. The 'anvil' shaped area of high variability seen to occur in this area [Figure 5 and more clearly in Figure 7] is mimicked by the locations of relatively large features present in Figure 13 [both negative and positive anomalies, cyclonic and anticyclonic eddies respectively].

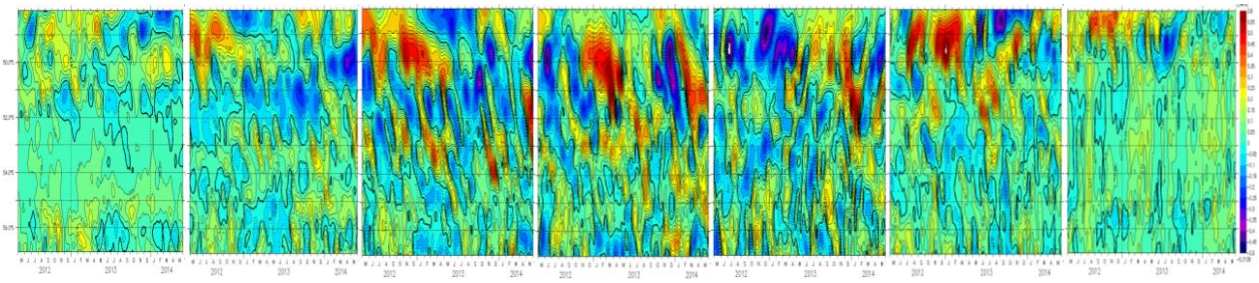

Figure 13 – A side-by-side view of 7 meridional Hovmöller analyses of the merged sea level anomaly for the longitudes: 25.4°E, 27.4°E, 28.4°E, 29.4°E, 31.4 °E, 34.4°E and 39.9°E, between the 48°S - 57°S, dated from 1 May 2012 to 31 May 2014. Blue to purple areas represent negative anomalies [cyclonic eddies] and yellow to red areas depict positive anomalies [anticyclonic eddies]. The SSHA scale is to the right in metres. Note: For the purposes of a west-east analysis of how the mesoscale features differ zonally across the southward eddy corridor, the 7 hovmoller plots [Figure 15 – 21] have been narrowed and repeated, in a filmstrip style, for ease of visual reference.

Overall, the population of negative anomalies during the 2 year period was higher than that of the positive features. However, what needs to be stressed here is that the population of positive anomalies south of 52°S [and within the region of the southward eddy corridor] is higher than the negative anomalies. What was also noted was that, of these features within the corridor, the positive anomalies are relatively larger in amplitude than their negative counterparts. These larger positive anomalies or anticyclonic features are formed as a result of the prominent circulation pattern of the area: the southward meander of the southern branch of the APF.

The general amplitudes of the features waxed and then waned from west to east. The positions of the larger amplitudes, typically above 52°S, mimic the route between the Sub-Antarctic Front and the Antarctic Polar Front [the area between the pink and red frontal bands in Figure 8] as it flows over the SWIR. The features clearly show that the variability between the SAF and APF is of a higher order than that between the other ACC fronts found further south.

Through the examination of the above series of Sea Surface Height Anomaly [SSHA] longitude-time Hovmöller plots, the recent western and eastern boundaries of the eddy corridor become apparent. Using the SSHA data for the particular day of the 16th April 2014, Figure 14 was created to show the meridional boundaries of the corridor and the positions of the mesoscale eddies within the corridor.

The projected meridional length of the southward eddy corridor, defined by Ansorge et al. (2015), was from 48°S to 57°S. Figure 14, the sea surface anomaly schematic of the area covered by the corridor on a specific day of the 2014 Marion Island Relief Cruise [MIRC2014], shows that the north and south borders closely agreed with those of Ansorge et al. (2015), with a few anomalies present south of 57°S. This further southward progression is rare, a possible explanation of this exception would be that the features which move this far south could have merged vortexes with other positive features in order to gain enough angular momentum to relocate south of 60°S (Sangrà et al., 2005).

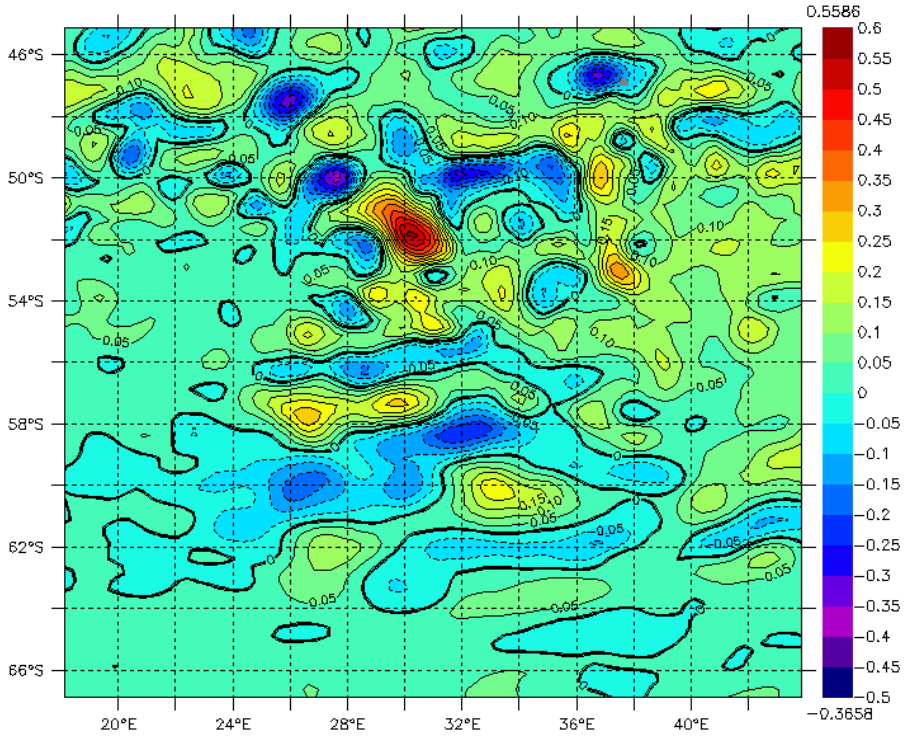

Figure 14 – A map of sea surface height anomaly [SSHA] over the region of interest from all available satellites on 16 April 2014. The SSHA scale is to the right [metres]. Blue to purple areas represent negative anomaly values [cyclonic eddies] and yellow to red areas depict positive SSHA values [anticyclonic eddies].

Note: For ease of discussion the above image is a repeat of an earlier image – Figure 11

The above figure shows that there was a distinct lack of anomalies south of 62°S and west of 26°E. The border separating the area of weak and strong mesoscale activity corresponds to the distribution of the southern boundary of the ACC [SACCF], shown by the blue line in Figure 8. What is also seen, is an area of

weakly defined positive anomalies east of 36°E; this illustrates the increase in mesoscale activity which had not yet formed individual mesoscale anticyclonic eddies. By observing the enlarged versions of the 7 individual Hovmöller transects [Figures 15 – 21], the boundaries of the southward flux of mesoscale eddies become clearer, especially how and where these features are advecting.

Figure 13 repeatedly shows the presence of large anticyclonic features forming close to the ABFZ of the SWIR, between 48° and 52°S. Figure 14 similarly shows the presence of a large positive anomaly [centred over 30°E, 52°S]. What may be happening is that these large anomalies are distorting and spawning smaller anticyclonic eddies which shift south through the corridor. Again, the assessment of the individual Hovmöller transects will shed light on how these features are advecting.

4.1.2 - INDIVIDUAL HOVMÖLLER PLOT ASSESMENTS

TRANSECT 1 – 25.4°E

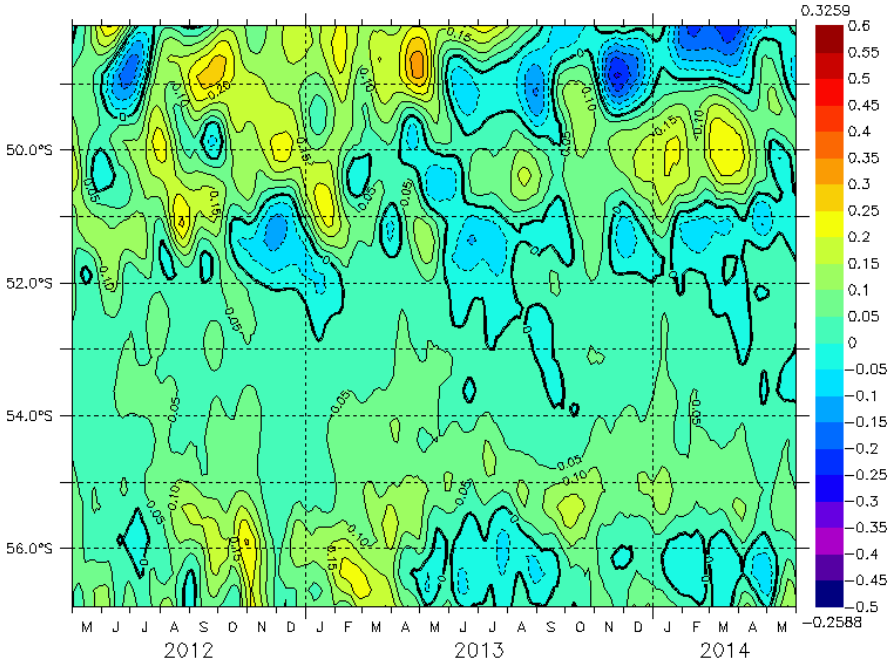

Figure 15 – A meridional Hovmöller analysis of the merged sea level anomaly for the 48°S - 57°S section of 25.4°E from May 2012 to May 2014. Blue to purple areas represent negative anomaly values [cyclonic eddies] and yellow to red areas depict positive anomaly values [anticyclonic eddies]. The SSHA scale is to the right in metres. Note: there are no anomalies shifting between 52°S and 55°S in the image.

The first Hovmöller plot [Figure 15] was situated west of the corridor at 25.4°E, between 48°S and 57°S. There appears to be a disconnect between features seen north of 52°S and anomalies found further south at 55°S. In the figure above, there appears to be no anomalies extending southwards. It is likely that the areas of variability along these latitudes are associated with the frontal bands of this region [APF and SACCF].

TRANSECT 2 - 27.4°E

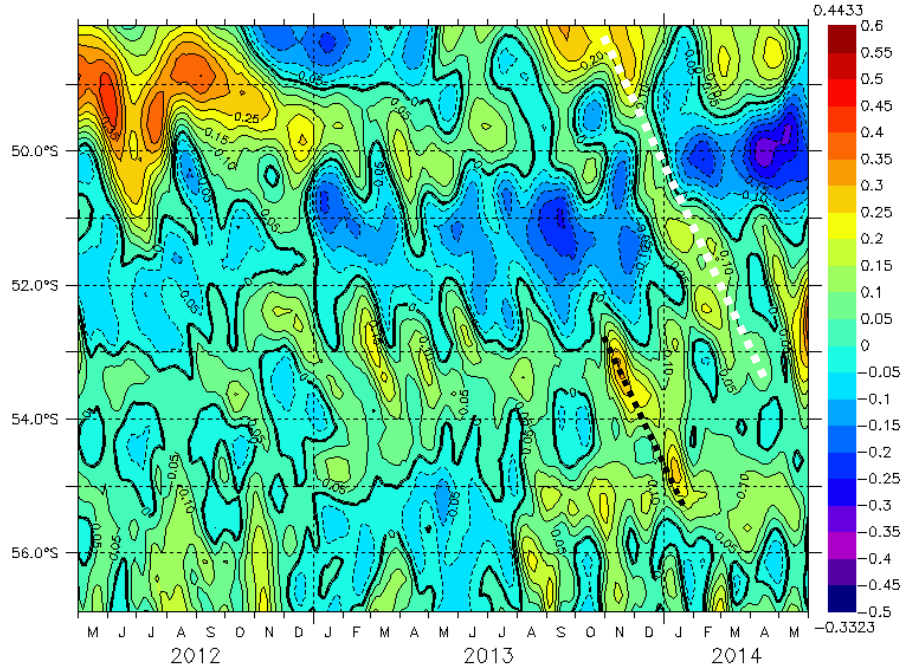

Figure 16 – A meridional Hovmöller analysis of the merged sea level anomaly for the 48°S - 57°S section of 27.4°E from May 2012 to May 2014. Blue to purple areas represent negative anomaly values [cyclonic eddies] and yellow to red areas depict positive anomaly values [anticyclonic eddies]. The SSHA scale is to the right in metres. There are short lived positive features between 52°S and 55°S in the image. Two southward anticyclonic eddy trajectories are marked by dotted lines.

The second Hovmöller plot [Figure 16] appears to show the western extreme of the southward extending anticyclonic eddy corridor at 27.4°E, between 48°S and 57°S. In this image many relatively small positive features began to ridge southward, which shows that, in contrast to the previous transect, positive anomalies appear to move southwards through the region. One noticeable example of this in Figure 16 is shown by a black dotted line. This short-lived positive feature began its track south November 2013, with a maximum sea surface anomaly of between 0.3 and 0.35m north of 53°S. This feature reduced in amplitude [averaging at 0.25m] and shifted south passed 55°S by March 2014.

What can also be noted from the figure above, is that, despite features forming north of 50°S, only one distinct mesoscale eddy appears to have shifted south [shown by a dotted white line in Figure 16]. This positive feature began its track south November 2013, with a maximum sea surface anomaly of between 0.25 and 0.3m north of 48°S. This feature reduced in amplitude [averaging at 0.15m] and shifted south passed 54°S by the end of the Hovmöller plot timeline.

TRANSECT 3 – 28.4°E

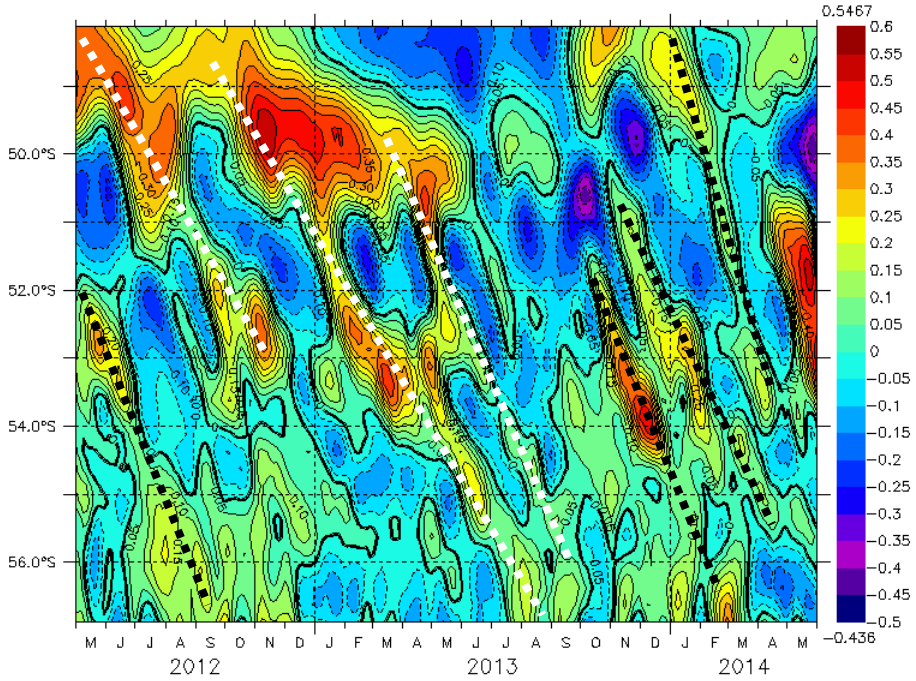

Figure 17 – A meridional Hovmöller analysis of the merged sea level anomaly for the 48°S - 57°S section of 28.4°E from May 2012 to May 2014. Blue to purple areas represent negative anomaly values [cyclonic eddies] and yellow to red areas depict positive anomaly values [anticyclonic eddies]. The SSHA scale is to the right in metres. There are seven positive features shifting south between 50°S and 56°S in the image, marked by dotted lines. The negative features are disjointed and shorter than their positive counterparts. There is a relatively large positive feature which remains at 50°S from the start of the Hovmöller plot until July 2013. The positive features during this time period appear to have spawned from this quasi-permanent positive anomaly.

The third Hovmöller plot [Figure 17 shows the mesoscale activity within the corridor along the 28.4°E longitude, between 48°S and 57°S. Similar to Figure 16 above, a strong positive feature [averaging at 0.45m in SSHA] was seen to be present at 49°S, and existed from before May 2012 up until the start of 2013. From early 2013 this large positive feature had advected south to about 50°S until June 2013, when it dissipated.

Figure 17 also shows seven occurrences where anticyclonic eddies had shifted south [shown by dotted lines], a few as far as 56°S. Three of these anticyclonic eddies [white dotted lines] appear to have spawned from the large, previously mentioned, positive anomaly, two of which shifted south past 56°S. Separate from this eddy spawning, four other positive anomalies appear to have shifted south [shown by black dotted lines]. These five features are relatively smaller in size and amplitude than the earlier three.

What needs to be noted is that there are a few negative features which appear to have shifted south. However, the overall southward progression distance of these relatively small negative features are found between 49°S and 54°S and only last five months. Therefore, the displacement of the negative features was less, and they were also shorter lived when compared to their positive counterparts.

TRANSECT 4 – 29.4°E

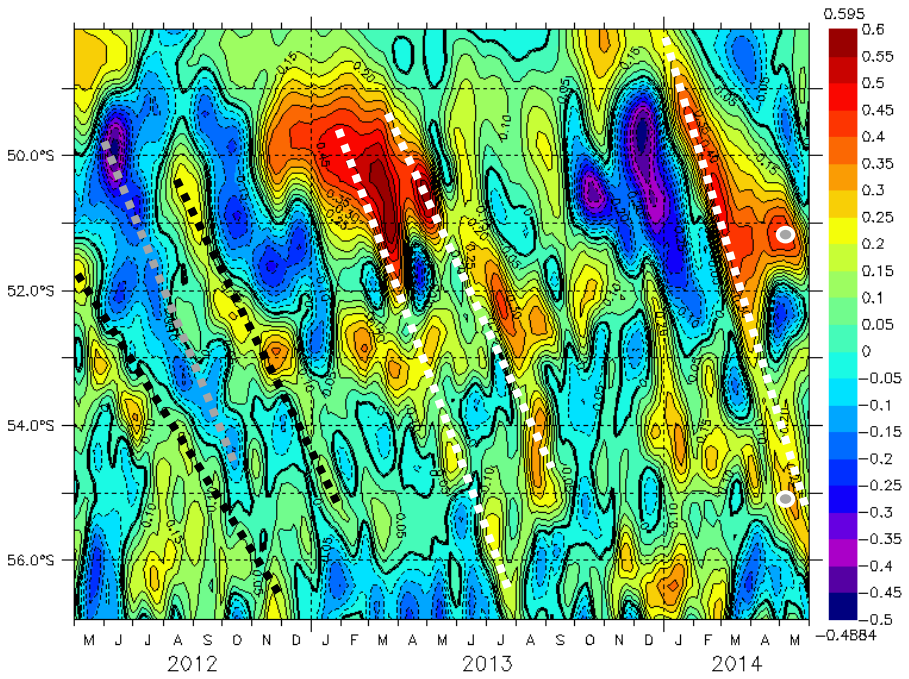

Figure 18 – A meridional Hovmöller analysis of the merged sea level anomaly for the 48°S - 57°S section of 29.4°E from May 2012 to May 2014. Blue to purple areas represent negative anomaly values [cyclonic eddies] and yellow to red areas depict positive anomaly values [anticyclonic eddies]. The SSHA scale is to the right in metres. There is a relatively large positive feature, which remains centred at 50°S from November 2012 to July 2013, and then another appears in January 2014 in the same position. The positive diagonal feature which initiates in January 2014, shows the southward trajectory of an anticyclonic eddy which was sampled during the 2014 Marion Island Relief Cruise. The two anticyclonic eddies which were sampled during the 2014 Marion Island Relief Cruise are shown by grey dots with white outlines. Five southward anticyclonic eddy trajectories are marked by dotted white and black lines. One southward negative eddy trajectories is marked by a grey dotted line.

The fourth Hovmöller plot [Figure 18] shows the mesoscale activity within the corridor along the 29.4°E longitude, between 48°S and 57°S. In this image, two strong positive features were seen to be present between 48°S and 52°S; the first lasting from November 2012 to June 2013, with a maximum SSHA of over 0.55m, and the second from October 2013 up until the end of the Hovmöller plot timeline in May 2014, with a maximum SSHA of over 0.45m. This image shows five distinct occurrences where anticyclonic eddies shifted south to as far as 55°S if not further [shown by dotted lines]. Three of these anticyclonic eddies originated from the two large positive features just mentioned, shown by white dotted lines. The other two are marked by black dotted lines and are generally smaller in size and have, on average, amplitudes of 0.25m.

By timeline, the first southward eddy trajectory seen in this plot [left black dotted line] was the anticyclonic eddy which began May 2013, at 52°S, and progressed south, passing 56°S by early November 2013. The second prominent southward eddy trajectory seen in this plot [right black dotted line] was the anticyclonic eddy which began August 2013, at 50.5°S, and progressed south until it dissipated at 55°S by the end of 2012. The third prominent southward eddy trajectory was the large positive anomaly at 50°S [middle white dotted line], which began late in 2012 and progressed south to 55°S by early September 2013. The fourth prominent southward eddy trajectory was the anticyclonic eddy which began early in January 2014 [far right white dotted line], at 52°S, and progressed south past 56°S by the end of March 2014. The fifth southward trajectory seen in this image has, as its origin, the second large positive feature of Figure 18

which formed above 48°S late in 2013. This large feature shifted south to 51°S by March 2014, then wedged southward, and a smaller positive feature pinched off from it during April. This smaller anticyclonic feature travelled south to 55°S by the end on the Hovmöller timeline. The initial large positive anomaly, from which this southward eddy pinched off, remained at 51°S up until the end of the Hovmöller plot timeline in May 2014.

As previously mentioned, the second large positive anomaly centred over 51°S, and remained in this position between March and May 2014. Since this feature did not shift, it retained its hydrographic circumstance. However, the positive eddy which was shed by this large feature moved south [far right white dotted line], changing its hydrographic circumstance, and in doing so would have been subjected to hydrographic evolution. This smaller positive feature therefore warranted the title of 'mature' eddy [marked by a grey dot], during the MIRC2014. In contrast, the initial large positive feature from which the mature eddy originated was given the title 'juvenile' eddy during MIRC2014 [also marked by a grey dot], as it remained in situ and so did not undergo changes in hydrographic circumstance. Thus, Figure 18 confirms that the origin of these two anticyclonic eddies [marked by grey dots; the juvenile and mature], sampled during the MIRC2014 eddy survey, is the ABFZ section of the SWIR. Objective three of this thesis features the hydrographic assessment of these two anticyclonic eddies.

In addition, the position of the anticyclonic 'juvenile' eddy appears to shift eastward during the two year sampling time period of this Hovmöller analysis. The position of this 'juvenile' eddy may be reliant on the ever fluctuating location of the fronts of the ACC relative to the ABFZ, specifically the Antarctic Polar Front.

Figure 18 also shows three large negative features which also appear to have shifted south to at least 54°S. Of these three, the most notable negative feature [marked by a grey dotted line] formed at 50°S, in June 2012, and had shifted south to 54.5°S by October 2012. These features initially have relatively high negative amplitudes [well over 0.4m] overall southward, however these depressions are reduced as they shift south. The progression distances of these negative features is found between 49°S and 54°S and each individually lasted for a period of five months. Therefore, compared to their positive counterparts, the negative features have shorter displacements and are shorter lived.

TRANSECT 5 – 31.4°E

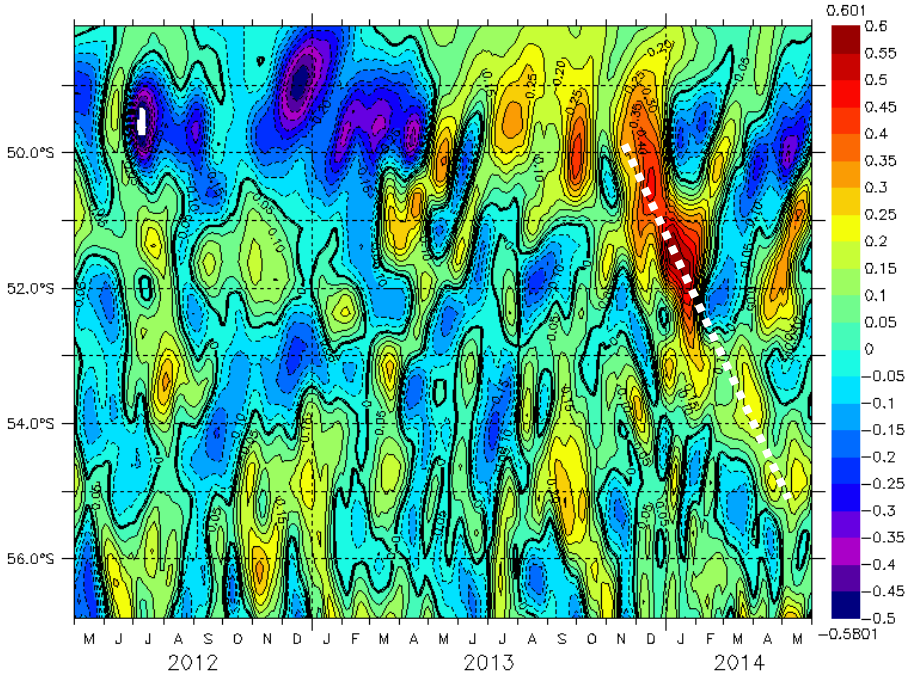

Figure 19 – A meridional Hovmöller analysis of the merged sea level anomaly for the 48°S - 57°S section of 31.4°E from May 2012 to May 2014. Blue to purple areas represent negative anomalies [cyclonic eddies] and yellow to red areas depict positive anomalies [anticyclonic eddies]. The SSHA scale is to the right in metres. It can be seen that a relatively large positive feature forms at 49°S in June 2013 and progressively shifted south until May 2014 [marked by a white dotted line].

The fifth Hovmöller plot [Figure 19] appears to show the eastern extent of the eddy corridor, along the 31.4°E longitude, between 48°S and 57°S. A relatively large positive feature [maximum amplitude being 0.6m], formed at 49°S during November 2013, is seen to have shifted south until May 2014 [marked by a white dotted line]. Apart from this single southward shifting anticyclonic eddy, it is clear that other positive and negative features are present in the image. However, they are not seen to have shifted as no distinct advection pattern can be observed from this image.

TRANSECT 6 – 34.4°E

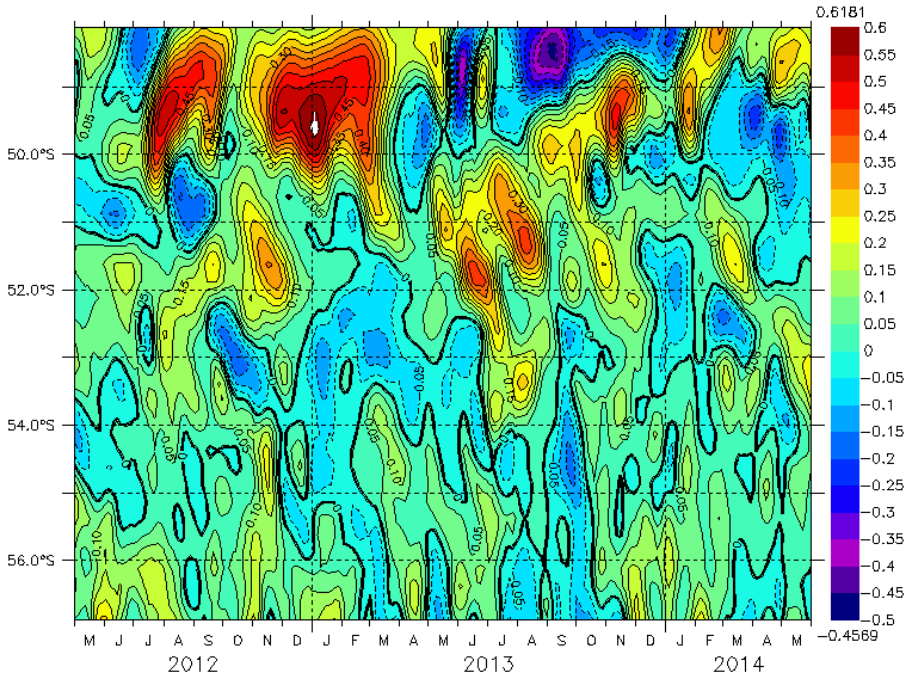

Figure 20 – A meridional Hovmöller analysis of the merged sea level anomaly for the 48°S - 57°S section of 34.4°E from May 2012 to May 2014. Blue to purple areas represent negative anomalies [cyclonic eddies] and yellow to red areas depict positive anomalies [anticyclonic eddies]. The SSHA scale is to the right in metres.

The sixth Hovmöller plot [Figure 20] shows the mesoscale eddy activity found east of the corridor, along longitude 34.4°E between 48°S and 57°S. Positive and negative features are present in the image, but are not seen to have shifted as no distinct advection pattern can be observed from this image. It can be surmised that there is a weak connection between features seen north of 52°S and anomalies found below 56°S. This shows that there were no positive anomalies which progressed south along the 34.4°E longitude. More positive features are forming at this section of the ABFZ compared to negative features, these positive features may have moved eastward toward the PEIs (Durgadoo et al., 2010). It is likely that the areas of high variability along these latitudes are associated with the divergence of the frontal bands of this region [APF and SACCF; seen by the spreading of red and grey lines in Figure 8].

TRANSECT 7 – 39.9°E

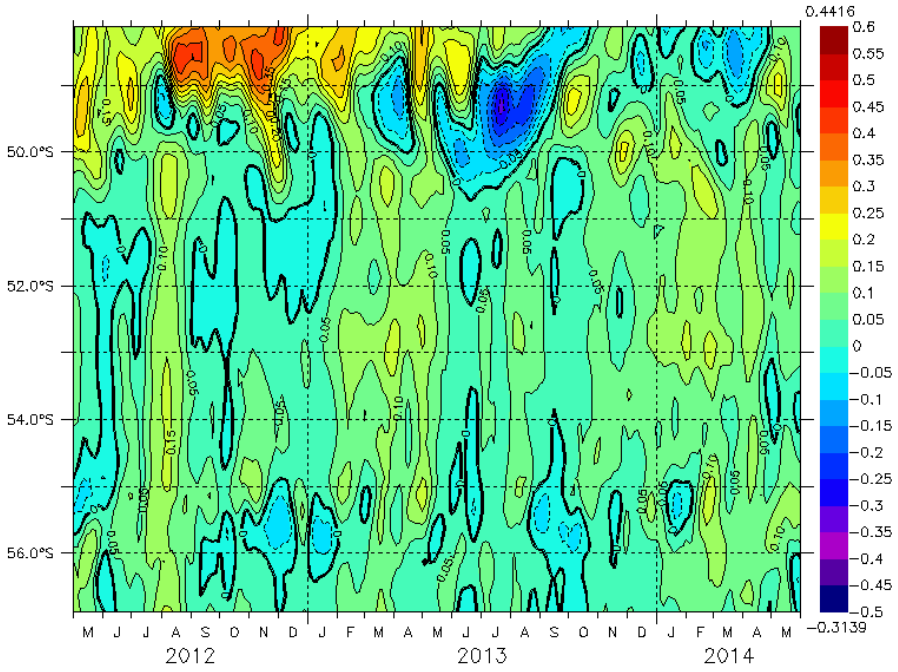

Figure 21 – A meridional Hovmöller analysis of the merged sea level anomaly for the 48°S - 57°S section of 39.9°E from May 2012 to May 2014. Blue to purple areas represent negative anomalies [cyclonic eddies] and yellow to red areas depict positive anomalies [anticyclonic eddies]. The SSHA scale is to the right in metres.

The seventh Hovmöller plot [Figure 21] was situated west of the southward anticyclonic mesoscale eddy corridor at 39.9°E between 48°S and 57°S. There appears to be a lack of eddies found south of 50°S: thus no anomalies have shifted south during the 2 year period. This image depicts the variability found east of the southward eddy corridor. As mentioned above, it is likely that the areas of high variability are associated with the divergence of the APF and SACCF; seen by the spreading of red and grey lines in Figure 8].

4.1.3 - OVERVIEW TOTAL ANTICYCLONIC MESOSCALE FEATURES FOUND TO ADVECT SOUTH

Ansorge et al. (2015) found that the rate at which southward propagating anticyclonic eddies were shifting south, over a 19.5 year period [1992 – 2012], was 1.4 eddies per year. From the above Hovmöller analysis of Figures 14 – 19, a total of 14 anticyclonic eddies were found to go south, which reaped a rate of 7 anticyclonic eddies travelling south per year between 2012 and 2014, most of which were confined between 28° and 30°E. This highly differing result may be a product of the sampling time period being significantly shorter than that of Ansorge et al. (2015).

Comparing the 1992-2012 timeline and the 2012-2014 timeline, there was a majority of anticyclonic eddies shifting south, as opposed to the number of cyclonic eddies. The life times of the southward eddies plotted in the 2012 – 2014 Hovmöller analysis was typically less than a year [approximately ten months or less], which is significantly longer than the standard four month life span found by Chelton et al. (2011). During the late stages of the mesoscale eddies found by Chelton et al. (2011) in this high latitude area, the signatures of these eddies may have been insignificant to be detected by their algorithm. Therefore, the

eddy terminations in the Chelton et al. (2011) data set may have been premature. Thus, the population of anticyclonic mesoscale eddies, which have been found to shift south from the APFZ into the AAZ, through this corridor, may have been aliased in previous survey.

4.2 - WHAT ARE THE TRAJECTORY CHARACTERISTICS OF THE 25 SOUTHWARD PROPAGATING MESOSCALE EDDIES?

In this section, the southward propagation tracks and scalar variables of the 25 anticyclonic eddies, identified from the Chelton et al. (2011) dataset between October 1992 and April 2012, are examined and discussed. In doing so, this section further supports and builds on from the previous section, which identified the differences across the area of high mesoscale activity, by looking at eddy tracks within this southward anticyclonic eddy corridor extending from north of the Antarctic Polar Front [APF] into the Antarctic Zone.

4.2.1 - OVERVIEW OF THE 25 SOUTHWARD EDDY PROPAGATIONS

All of the eddies studied [the blue tracks in Figure 9] were shown to form in close proximity to the Andrew Bain Fracture Zone [ABFZ] between 26° and 32°E and 49° and 52°S. These eddies generally followed the southern slope of the South West Indian Ridge [SWIR], though a single eddy [eddy 159817, the red track in Figure 20] was observed to deviate far to the east by having propagated further east into the Enderby Basin [34.45°E], in close proximity to the Conrad Rise. Figure 9 shows how the eddies follow the slope of the SWIR and there appears to be an area of constriction at ±28°E, 52°S before they meridionally spread out further south. This constriction is most likely due to the deflection in both the Subantarctic Front [SAF] and Antarctic Polar Front [APF] bands as they cross over the SWIR (Ansorge and Lutjeharms, 2003). Most eddy tracks terminated by 55°S, with just 8 eddies continuing further south. One eddy [the cyan track in Figure 22] propagated as far as 57.07°S, before retroflecting northwards and terminating at 56.39°S. When each of the 25 eddy trajectories were individually analysed, it was noted that there were five different types of track patterns: slope following, partial slope following, directly south, a southward track with a retroflection, and a southeast track pattern. An assessment of these 5 particular southward anticyclonic eddy types follows after this overview.

It could be surmised that - provided the eddies are deep enough and the laws of potential vorticity conservation apply - the depth of the features, which are destined to shift south, may be a deciding factor of the traits of its future trajectory. Shallower features may be entrained by the flow of the surrounding waters, while deeper features may be confined to the bathymetry over which they flow (Sutyrin et al., 2003; Sutyrin et al., 2009), as potential vorticity must remain constant (Pedlosky, 2013). A study of the strength of these features' geostrophic flow dynamics, may also affect the features' ability to resist the surrounding flow of the host waters. Thus, angular momentum could also impact the distance the eddy travels.

Another factor, which could influence future eddy trajectory, may be the position, along the Andrew Bain Fracture Zone [ABFZ], at which the feature commences its southward propagation. Past studies have shown that a large portion of eddies, formed as a result of the ABFZ influence on the ACC, travel east towards the Prince Edward Islands [PEIs] – so what forces this southward flux of anticyclonic eddies? Frontal positions and their specific jet strength at the time of eddy formation could be a strong influence

on the tracks directionality. Craneguy and Park (1999) proposed that eddy trajectories could be dependent of bottom velocities, where deep features with bottom velocities exceeding 3cm.s^{-1} were controlled topographically, whereas weaker velocities of shallower features were governed by surrounding frontal dynamics. As mentioned in the above results section 4.1, it could also be likely that the formation of these anticyclonic features, along these latitudes, is associated with the divergence of the frontal bands of this region [APF and SACCF] which is as a result of the ACC interacting with the Conrad Rise. Specifically, the explanation for the southward propagation of eddies is likely to be that the eddies become entrained in the southward extension of the ACC, particularly the southward deviation of the Southern Antarctic Circumpolar Front [SACCF] which is depicted by the grey line plotted in Figure 8.

4.2.2 - ASSESSMENT OF 5 SOUTHWARD ANTICYCLONIC EDDY TRACKS

The five anticyclonic eddy trajectories chosen represent the five distinct eddy subset track types found within the Chelton et al. (2011) dataset. These are the eddies numbered: 159817, 180229, 184852, 188503 and 191298; plotted in red, blue, magenta, cyan and green, respectively in Figure 22. These five subsets together depict the typical southward progression of eddies within the anticyclonic mesoscale eddy corridor. The remaining individual 20 eddy trajectory plots can be seen in Appendix B.

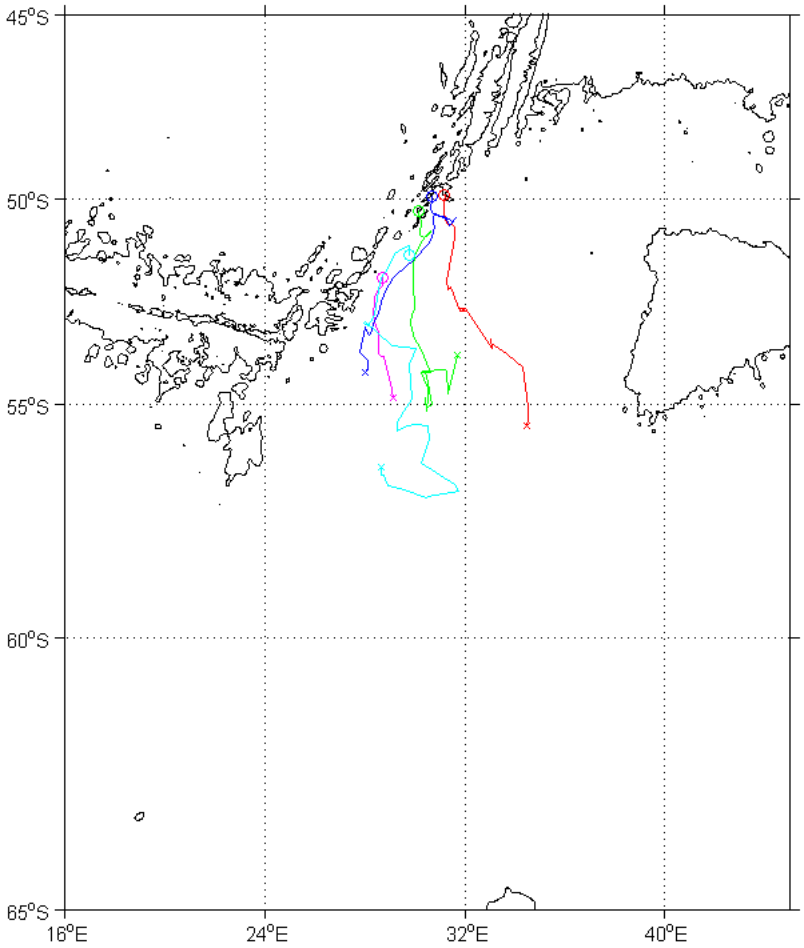

Figure 22 – Trajectory plots of the 5 anticyclonic eddies: 159817, 180229, 184852, 188503 and 191298 from Chelton et al. (2011) [red, blue, magenta, cyan and green, respectively]. These are five out of the 25 anticyclonic mesoscale eddies which were found to propagate south from the South West Indian Ridge by Ansorge et al. (2015). The bathymetric environment is presented by the 3500m isobath [shown by the black contour line]. A single trajectory consists of a starting position [demarcated with a 'o'], a track line and the termination position [symbolised by an 'x'].

Eddy 159817 [red track in Figure 22] had a track which lasted for 25 weeks, started further north than the other 25 eddies and was not confined to the slope of the ABFZ. This track headed towards the Conrad Rise. Eddy 180229 [blue track in Figure 22] was also confined, during its 30 week lifespan, to follow the contours of the ABFZ. Eddy 184852 [magenta track in Figure 22] shifted directly south during its lifespan of 17 weeks. Eddy 188503 [cyan track in Figure 22] had a relatively erratic southward track, lasting 35 weeks. This track involved partial slope following but was not completely directed by the slope of the ABFZ, as it deviated away and shifted east into the abyssal plain between the SWIR and the Conrad Rise. Eddy 191298 [green track in Figure 22] is also an example of a southward trajectory which included a retroflection after it had shifted past 55°S.

4.2.3 - SCALAR VARIATIONS OF THE 25 HISTORICAL ANTICYCLONIC MESOSCALE EDDIES

Durgadoo et al. (2010) explained that the decay of mesoscale eddies generally includes a waning in their rotation rates, a reduction in their sea surface height signature and a change in their temperature-salinity characteristics. The dataset created by Chelton et al. (2011) not only tracked global mesoscale eddies, but also monitored each eddies' radius for each data point of every eddy trajectory, the circum-average speeds [rotation rate at the circumference] and the sea surface height extremum [amplitude].

Plotting the scalar variables of the mesoscale eddies, along with the mean and standard deviation of the variables over time, allows for the fluctuations of these variables to be viewed as the eddy travels and ages. Figure 23 shows the scalar variables: Radius [km], Rotation rate at the circumference or Circum-average speed [$cm.s^{-1}$] and Sea Surface Height Signature or amplitude [cm] of each observation sequence number [each a sampling interval of seven days], for the 25 anticyclonic eddies found to travel south from the South West Indian Ridge, between 1992 and 2012, along with the respective means [shown in black] and the standard deviation [shown by the grey lines]. The longest lived eddy [no. 195740] lasted for over 55 observations [55 weeks], over 25 observations more than the other observed 24 southward anticyclonic eddies. In Figure 23 this observed eddy is shown by the yellow line, along with the 5 previously isolated eddies: 159817, 180229, 184852, 188503 and 191298 [red, blue, magenta, cyan and green, respectively]. After week 38, in all three scalar graphs, the mean merges with the yellow line of eddy no. 195740: from this point on, the line is striped yellow and black until ending at week 58.

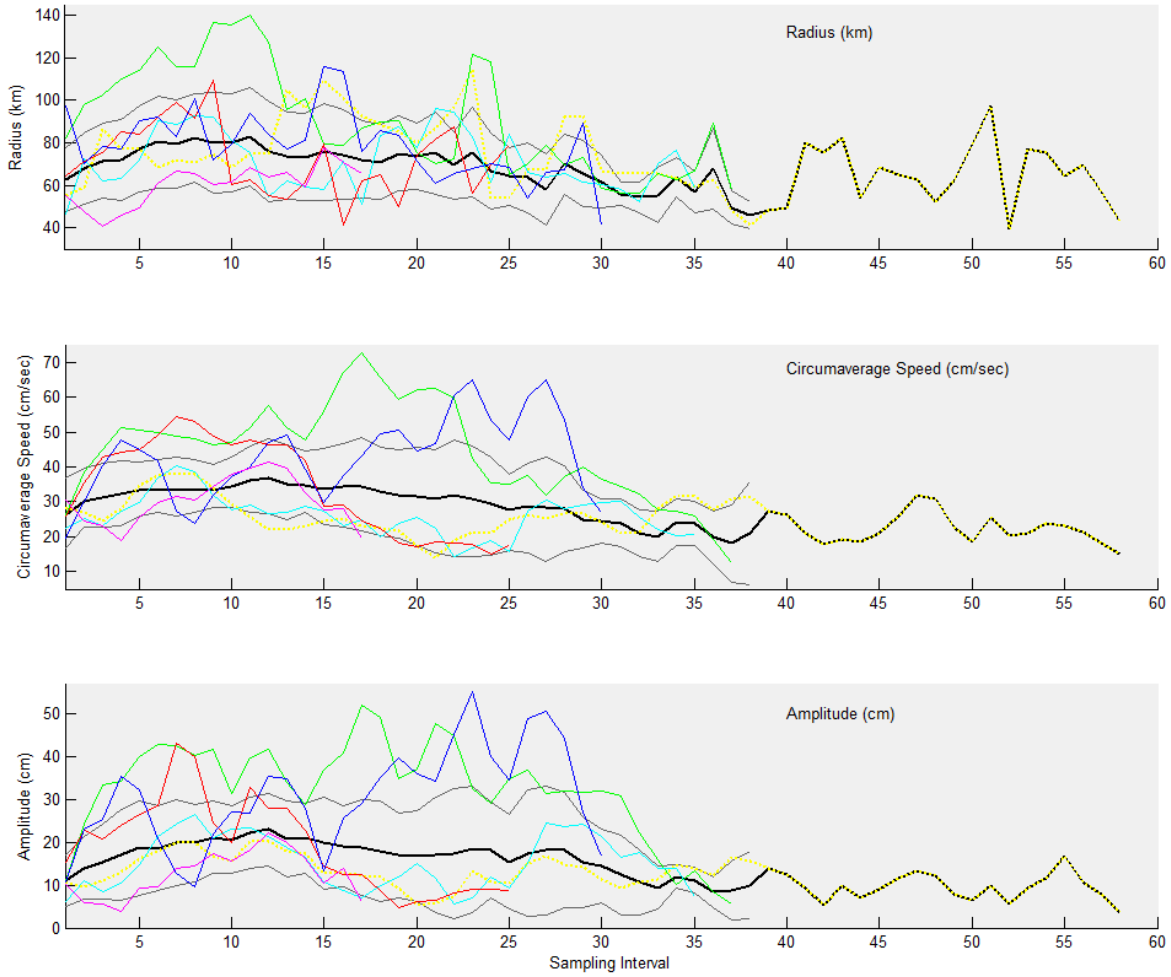

Figure 23 - Three line charts showing the scalar variables versus the sampling interval [a 7 day time step]: Radius [km], Rotation rate or Circum-average speed [cm.s^{-1}] and Sea Surface Height Signature or amplitude [cm]. The scalar property changes of 6 previously identified anticyclonic mesoscale eddies are plotted [159817, 180229, 184852, 188503, 191298 and 195740 - red, blue, magenta, cyan, green and yellow, respectively], along with the scalar mean of all the 25 anticyclonic eddies found to travel south from the South West Indian Ridge (Ansorge et al., 2015), between 1992 and 2012, [black] and with the ±standard deviation [grey].

From the contour of the three means it can be seen that, for the first twelve weeks, these eddies - on average - gradually grew in surface area and in rotation rates at the circumference and also in amplitude. For this initial period of time, the average radius grew from 63 to 80 km. Also, for this period of time, the average circum-average speed increased from 28 to 47 cm.s^{-1}. In addition, this initial period of time, the average eddy amplitude increased from 12 to 23 cm. From week thirteen until trajectory termination, there was a slow decline in diameter, rotation rate and amplitude [except for the longest lifetime eddy].

What was perceived from week 27 was that the means noticeably fluctuated more, in each plot. This was because, as there were less eddies with life-spans exceeding 27 weeks, there were fewer eddies contributing to the mean calculation. Thus, the latter part of the three means show more erratic behaviours. The range of deviation of the mean for the radius was approximately 30km; the range of deviation of the mean for the rotation rates at the circumference was 10 cm.s^{-1}; the range of deviation of the mean for the eddy amplitudes was close to 5cm.

Viewing the general manner by which the scalar variables change for the 6 isolated eddies [relative to the mean ± the standard deviation], what can be seen is that the spikes in radii are more pronounced than

those of amplitude and circum-average speed. This scalar spiking of radii could be reduced if the time step between each observation were to have been less than the seven day interval used by Chelton et al. (2011). Within the first fifteen observations, there was a high population of eddies, but by observation interval 13 the population had significantly decreased.

The yellow line serves the purpose of showing the scalar progression of a single eddy [eddy no. 195740] compared to the mean of the twenty five eddies. This eddy's scalar lines do not appear to consistently remain above or below the respective means, but straddles them. This meandering, which stays predominantly within the standard deviation range of the three plots, implies that the single eddy is typical of the southward propagating anticyclonic eddies as it closely follows the mean. The fluctuation is due to the positive mesoscale eddies being influenced by opposing geostrophic flows, particularly by the presence of negative features, which alter the positive eddies' sea surface shape, circumferential rotation speed and amplitude as they shift south. A similar fluctuating quality is seen in the results of the Hovmöller plot analysis earlier in this objective, in which features were seen to be continually expanding and contracting in size and amplitude.

CONFIDENCE OF THE 25 EDDY TRACK ANALYSIS

Apart from the anticyclonic eddies which propagated directly south [the red eddy track in Figure 20], the tracks of the southward advecting anticyclonic eddies typically followed the southern slope of the SWIR. Thus, the most common path of these anticyclonic eddies was not directly south as shown in the Hovmöller analysis, but curved towards the west, following the southern slope of the SWIR. This analysis has provided a more practical understanding of how the anticyclonic mesoscale eddies travel within this southward eddy corridor.

This southward movement of anticyclonic mesoscale eddies through the corridor could be allowing a cross barrier flux of heat, characteristic of the waters of the APFZ, to enter in to the Antarctic Zone. The in situ analysis [the next section] endeavours to show this. Thus, this southward movement of anticyclonic mesoscale eddies through the southward corridor, could have strong implications, as the oceanic heat flux south into the Antarctic region is responsible for controlling the mass balance of the Antarctic cryosphere, specifically the Antarctic ice sheet (Rintoul and Naveira Garabato, 2013).

Satellite based observations and analyses, such as in Objective 1 and 2, are unable to allude to the contents of these anticyclonic mesoscale features. These features with characteristically warmer temperatures within them need to therefore be investigated through in situ means.

4.3 - HOW ARE THESE MESOSCALE FEATURES STRUCTURED HYDROGRAPHICALLY?

Mesoscale eddies have been identified as one of the principal mechanisms for the meridional transport of heat, salt and biota across the strongly zonal Antarctic Circumpolar Current [ACC]. These mesoscale eddies of the SO modify the upper ocean layers biogeochemistry, while simultaneously moving biota southwards across from one zone of the ACC to another. A direct consequence of this southward translocation, is the role played by the eddies in the uptake of anthropogenic carbon dioxide [CO_2] (Ito et al., 2010). Furthermore, the heat supplied by the southward train of warm anticyclonic eddies, into the Antarctic Zone [AAZ], has been shown to alter the flux of surface heat sufficiently to impact sea ice concentrations and their distribution directly south of this region (Ansorge et al., 2015) [Figure 24]. Understanding the hydrographic contents of these southward propagating anticyclonic eddies is fundamental for a better understanding of the role these features play in relocating hydrographic properties across frontal zones.

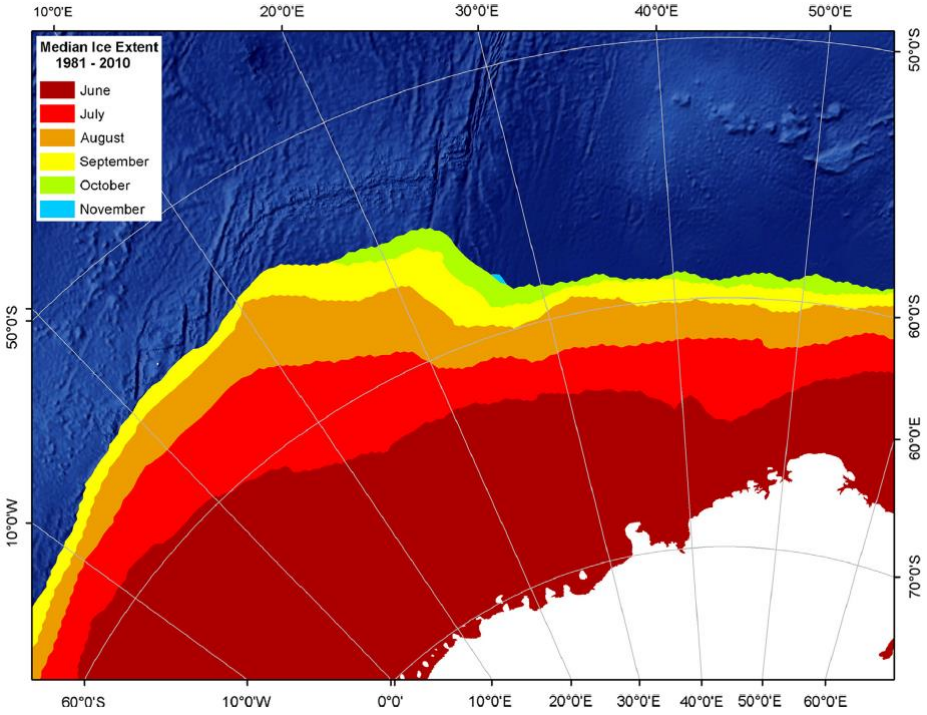

Figure 24 – The median monthly ice extent [0 – 90%], for the period 1981 – 2010. Note: the region south of the Andrew Bain Fracture Zone section of the South West Indian Ridge [25° - 35°E], has less sea ice extent than the region to the west. (Ansorge et al., 2015)

This section uses in situ oceanographic data, collected during the MIRC2014 [Section 3.3], to compare the thermal structural and saline structural differences between two anticyclonic eddies observed within the southward corridor of warm anticyclonic eddies found to be moving into the AAZ. This section constitutes an analysis of a juvenile anticyclonic mesoscale eddy and a mature anticyclonic mesoscale eddy. For the juvenile anticyclonic eddy; one temperature section, one salinity profile and a temperature versus salinity plot are shown and described [Figures 25 and 26]. For the mature anticyclonic eddy; two temperature sections, two salinity profiles and two temperature versus salinity plots are shown and described [Figures 27 – 30].

The temperature versus salinity [T/S] plots demonstrate the water masses present within the two sampled anticyclonic mesoscale eddies. Typical water masses found in the region of the Antarctic Polar Frontal Zone [APFZ] are: Sub-Antarctic Surface Water [SASW], Antarctic Surface Water [AASW], Antarctic Intermediate Water [AAIW], Winter Water [WW], Circumpolar Deep Water [CDW], and Antarctic Bottom Water [AABW] (Orsi et al., 1995).

Due to the SASW mass being in contact with the atmosphere, the SASW has a relatively high temperature value. Due to the high amount of precipitation in the area of the Sub-Antarctic Polar Frontal Zone [SAPFZ], this water mass also has low salinity values. The Modified SASW [M-SASW] is SASW which has been isolated due to the presence of cyclonic eddies and has relatively lower salinities at the surface. Due to the downwelling dynamics within anticyclonic eddies, the depth of AAIW is relatively deeper in the centre of an antcyclonic eddy and is conversely shallower on the exterior. This difference in depth allows for the differences in salinity and temperature values between the station profiles inside and outside of an anticyclonic eddy. AABW and CDW, with their low temperature ranges and high salinities, are found at the bottom of every station - AABW being the most dense lies below the CDW. For each transect there was one station, at the end of each transect, which depicts the water column stucture which would occur naturally in this region, if there were no mesoscale eddies present: it would be a cool column with a strong subsurface temperature minimum layer, commonly termed Winter Water (Park et al., 1997).

4.3.1 - JUVENILE ANTICYCLONIC MESOSCALE EDDY: AN IN SITU ANALYSIS

TRANSECT 1

A West-East survey of a juvenile anticyclonic mesoscale eddy was conducted. This feature was found to have formed as a result of the fractured nature of the SWIR inducing high mesoscale variability in the ACC [Section 4.1]. This eddy centred over 30°E, 52°S [Figure 11] and remained in this position between March and May 2014. Since this feature did not relocate during its observed lifetime, it retained its hydrographic signature. Therefore, this feature provides detail of the hydrographic contents of an eddy prior to propagation southward through the eddy corridor.

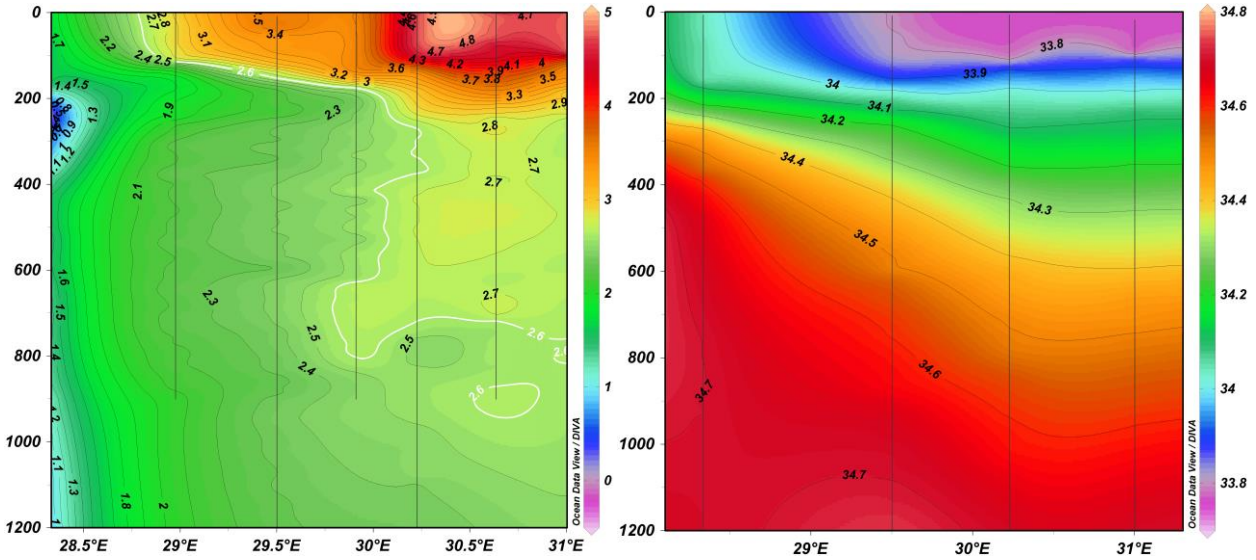

Figure 25 – West-East temperature [left] and salinity [right] sections of a juvenile anticyclonic eddy, close to the Andrew Bain Fracture Zone. The temperature range [in °C] is shown by the red to lilac colour bar found on the right of the temperature profile. A white 2.5°C isotherm defines the bulk of the sampled mesoscale eddy. The temperature maximum of the juvenile eddy is found at the surface, above 100m. The salinity range is shown by the red to lilac colour bar found on the right of the salinity profile, with units of psu. There is a 100m pool of relatively low salinity water at the surface and, below this, altering stratification from 100m to approximately 1200m. Below 1200m, the water has salinity above 34.7psu. The black vertical lines on both profiles mark the station locations: the temperature section contains both XBT casts [down to 900m] and CTD casts [3000+m].

Figure 25 is of the West-East temperature section, along 52°S from 28.5° to 31°E, and observes the western half of the juvenile anticyclonic eddy. For a visual reference for this section, the juvenile anticyclonic eddy boundary is demarcated by a thick white line; the 2.6°C isotherm. This specific isotherm was chosen to highlight the general shape of the mature feature relative to the juvenile feature. The majority of the heat of this feature is contained in the top 150m of the eddy, which has a relatively warm centre compared to its APFZ environment. Despite the majority of the heat being confined to the surface, the 2.5°C isotherm shows that the eddy's thermal structure has a 'T' shape to it. Isotherms are typically depressed in the centres of anticyclonic eddies; this downwelling of warm water exceeded 1200m within the centre of this feature. The warm area below 200m is thermally uniform [approximately 2.6°C]. It was also noted that the surface pool of high temperature of the juvenile eddy does not span the whole width of the eddy.

The salinity section of the juvenile anticyclonic eddy shows that there is stratification of the water, within the eddy, down to 1200m. The individual isohalines have altering haloclines, signifying a stratification which is not completely uniform. This stratification ranges from a 100m pool of relatively low salinity [<34psu] at the surface increasing to >34.7psu at 1200m, as Circumpolar Deep Water is encountered. As with the surface pool of high temperature, the surface pool of low salinity of the juvenile eddy also does not span the whole width of the eddy.

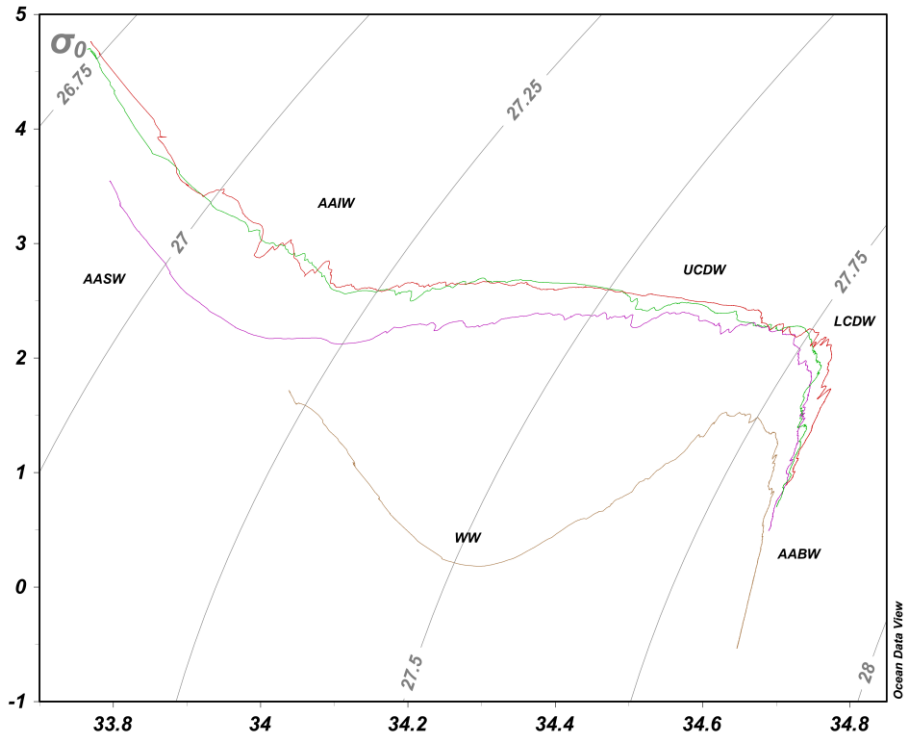

Figure 26 – A Temperature/Salinity schematic of the four Conductivity, Temperature and Depth [CTD] stations of Transect 1, across a juvenile anticyclonic mesoscale eddy, close to the Andrew Bain Fracture Zone. Salinity [x-axis] is in practical salinity units [psu], while Potential temperature [y-axis] is in °C. From west to east: CTD station 1 [shown in beige] to the west of the juvenile anticyclonic eddy, CTD station 2 [shown in magenta] the west of the juvenile anticyclonic eddy's core, CTD station 3 [shown in green] just west of the centre of the juvenile anticyclonic eddy and CTD station 4 [shown in red] positioned just east of the centre of the juvenile anticyclonic eddy. From surface to bottom, the water masses present within the eddy are labelled; Antarctic Surface Water [AASW], Antarctic Intermediate Water [AAIW], Winter Water [WW], Upper and Lower Circumpolar Deep Water [UCDW; LCDW] and Antarctic Bottom water [AABW].

In Figure 26, the beige station profile [west of the juvenile anticyclonic eddy], shows that waters surrounding the eddy are typical of the Antarctic zone [AAZ], which includes the presence of the significantly cooler Winter Water mass. The other profiles [the purple, green and red profiles] show that waters contained within the juvenile anticyclonic eddy are characteristic of the APFZ. The profiles which depict the internal structure of the juvenile eddy are not completely smooth, nor do they show that there is a presence of interleaving between the water masses contained within the transected eddy. This is in contrast to what can be seen in Figure 28, which shows the internal structure of the mature eddy.

4.3.2 - MATURE ANTICYCLONIC MESOSCALE EDDY IN SITU ANALYSIS

TRANSECT 2

A North-South survey of a mature anticyclonic mesoscale eddy, found to have shifted southwards along the eddy corridor [Section 4.1] was conducted. This feature formed as a result of the fractured nature of the SWIR inducing high mesoscale variability in the ACC. In shifting south, this anomaly, centred over 30°E, 57.3°S [Figure 11], had advected south, and changed its hydrographic circumstance. Therefore, this feature provides the hydrographic contents of an eddy which had propagated southward into the AAZ.

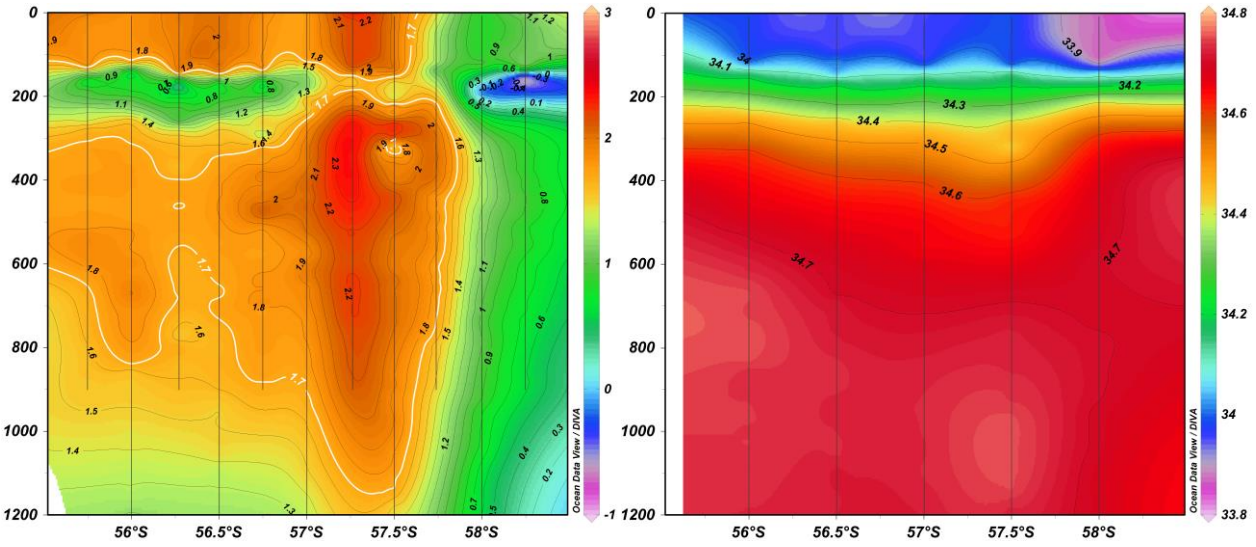

Figure 27 - North-South temperature [left] and salinity [right] sections of a mature anticyclonic eddy, close to the Andrew Bain Fracture Zone. The temperature range [in °C] is shown by the red to lilac colour bar found on the right of the temperature profile. A white 1.7°C isotherm defines the bulk of the sampled mesoscale eddy. The temperature maximum of the mature eddy is found below 200m. The salinity range is shown by the red to lilac colour bar found on the right of the salinity profile, with units of psu. There is a 100m pool of relatively low salinity water at the surface. The black vertical lines on both profiles mark the station locations: the temperature section contains both XBT casts [down to 900m] and CTD casts [3000+m].

Figure 27 includes the North-South temperature section, along 29.5°E from 55.7° to 59.2°S, profiling a mature anticyclonic eddy. For a visual reference, the mature anticyclonic eddy is demarcated by a thick white line [1.7°C isotherm]. It can be seen, from Figure 27, that this eddy contains the bulk of its heat within 220m and 500m. The temperature section shows that thermal interleaving has occurred between 150m to 210m; this is where Winter Water has become entrained into the boundaries of the anticyclonic eddy and altered the water properties at that level. Other than the thermal interleaving, the 1.7°C isotherm shows that the eddy has an elongate shape, with a narrow surface signature, and is thermally uniform down to 1200m.

The North-South salinity section of the mature anticyclonic eddy shows that there is stratification of the water in the top 300m of the water column. This stratification ranges from a 100m pool of relatively low salinity [<34psu] at the surface increasing to >34.7psu at 1200m as Circumpolar Deep Water is encountered. It is also notable that the surface pool of low salinity of the juvenile eddy spans the whole width of the eddy, contrasting with that of the juvenile anticyclonic eddy.

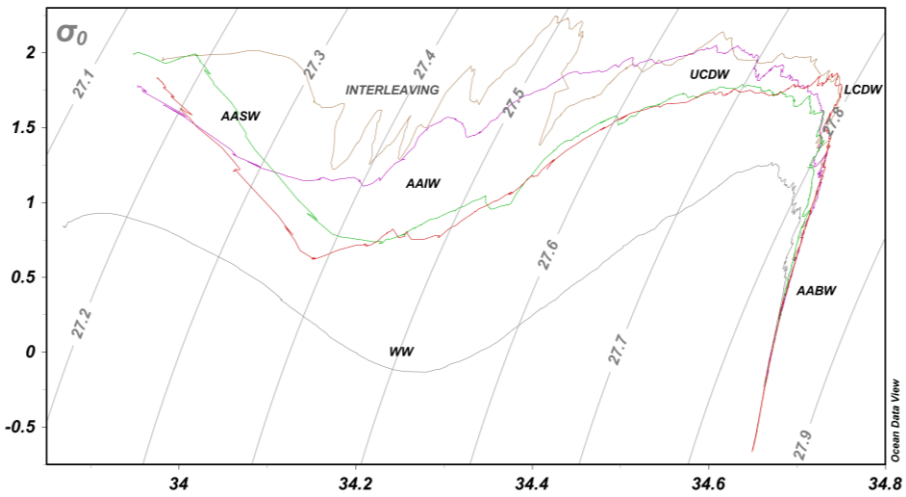

Figure 28 – A Temperature/Salinity schematic of the five Conductivity, Temperature and Depth [CTD] stations of Transect 2, across a mature anticyclonic mesoscale eddies south of the Andrew Bain Fracture Zone. Salinity [x-axis] is in practical salinity units [psu], while Potential temperature [y-axis] is in °C. CTD station 5 positioned north of the mature anticyclonic eddy [shown in red], CTD station 6 positioned north of the mature anticyclonic eddy [shown in green], CTD station 7 positioned at the western extent of the mature anticyclonic eddy [shown in magenta], CTD station 8 positioned at the centre of the anticyclonic eddy [shown in beige] and CTD station 9 positioned east of the mature anticyclonic eddy [shown in grey].

In Figure 28, the grey station profile [south of the mature anticyclonic eddy], shows waters characteristic of the surrounding AAZ. The red and green station profiles show that a cyclonic mesoscale eddy was present north of the mature anticyclonic eddy. These two station profiles show that contained within the cyclonic feature was waters which were characteristic of the APFZ, which have clearly been modified during this eddies displacement south. The magenta and beige, show that the waters within the mature anticyclonic eddy which were characteristic of the APFZ, have been modified during this eddies displacement south. The stations within the mature anticyclonic eddy, particularly the 8th station profile [beige] show the severe interleaving this feature has experienced. These jagged profiles are dissimilar to the station profiles seen within the juvenile anticyclonic eddy [Figure 26], which are smoother.

TRANSECT 3

A west-east survey of a mature anticyclonic mesoscale eddy, found to have shifted southwards along the eddy corridor [Section 4.1] was conducted. This feature formed as a result of the fractured nature of the SWIR inducing high mesoscale variability in the ACC. In shifting south, this anomaly, centred over 30°E, 57.3°S [Figure 11], had advected south, and changed its hydrographic circumstance. Therefore, this feature provides the hydrographic contents of an eddy which had propagated southward into the AAZ.

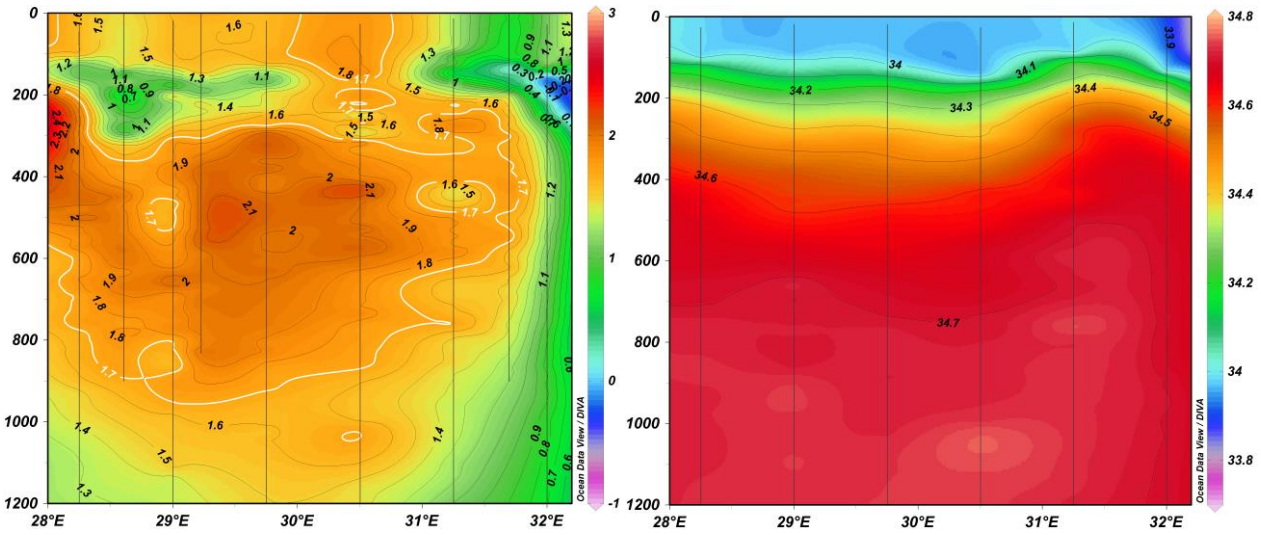

Figure 29 – West-East temperature [left] and salinity [right] sections cutting through a mature anticyclonic eddy. A white 1.6°C isotherm defines the bulk of the sampled mesoscale eddy. The temperature range is shown by the red to lilac colour bar found on the right of the temperature profile. The salinity range is shown by the red to lilac colour bar found on the right of the salinity profile. There is a 100m pool of relatively low salinity water at the surface and, below this, altering stratification from 100m to approximately 700m. Below 800m, the water has a salinity value above 34.7psu. The black vertical lines on both profiles mark the station locations: the temperature section contains both XBT casts [down to 900m] and CTD casts [3000m].

Figure 29 is of the West-East temperature section, along 57.5°S from 28.2°E to 32°E, cutting through a mature anticyclonic eddy. For a visual reference, the mature anticyclonic eddy is demarcated by a thick white line [1.7°C isotherm]. In this section the bulk of this features' warmth is contained below 200m and extends down to 1200m. This temperature section shows partial thermal interleaving occurring between 150m to 210m; this is where Winter Water has become weakly entrained into the anticyclonic eddy and gradually altered water properties at this depth. The width of the feature is not vertically uniform; the width is narrower at the surface, with a wider sub-surface bulge below the Winter Water interleaving.

When comparing the temperature sections between the North-South and West-East transects of the mature anticyclonic eddy, what was clear is the relatively cooler [an approximate difference of 0.2°C] North-South thermal structure compared to that of the West-East transect. As these two transects were sampled within two days of each other, such a significant loss of heat is unlikely to have occured. This difference is actually as a result of the West-East transect not transecting directly through the core of the mature anticyclonic, but just to its south.

The West-East salinity section of the mature anticyclonic eddy, in Figure 29, shows that stratification of the water is within only the top 600m of the water column. This stratification ranges from a 100m layer of relatively low salinity [<34psu] at the surface, increasing to >34.7psu from 700m down was, as Circumpolar Deep Water is encountered. What was also noted was that the surface pool of low salinity of the mature eddy spans the whole width of the eddy, in contrast to that of the juvenile anticyclonic eddy.

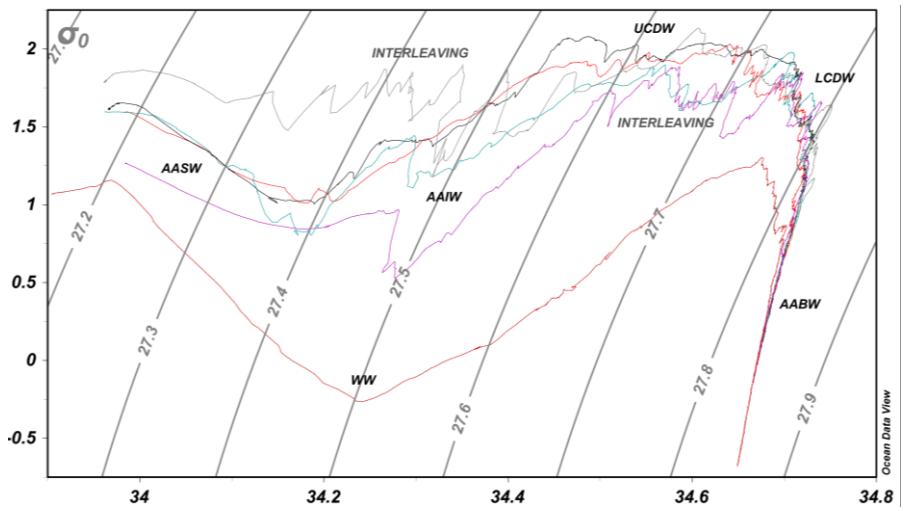

Figure 30 – A Temperature/Salinity schematic of the six Conductivity, Temperature and Depth [CTD] stations of Transect 3, zonally across a mature anticyclonic mesoscale eddy found south of the Andrew Bain Fracture Zone. Salinity [x-axis] is in practical salinity units [psu], while Potential temperature [y-axis] is in °C. From west to east: CTD station 10 positioned west of the sampled mature anticyclonic eddy [shown in red], CTD station 11 positioned at the western extent of mature anticyclonic eddy [shown in turquoise], CTD station 12 positioned near the centre of mature anticyclonic eddy [shown in black], CTD station 13 positioned also near the centre of mature cyclonic eddy [shown in grey], CTD station 14 positioned at the eastern extent of mature anticyclonic eddy [shown in purple] and CTD station 15 positioned at east of the mature anticyclonic eddy [shown in red-brown]. The grey and magenta station plots show interleaving to be present at the mature eddies' boundaries.

In Figure 30, the red-brown station profile [east of the mature anticyclonic eddy], shows waters characteristic of the surrounding AAZ. The other station profiles [red, turquoise, black, grey and red-brown] show that the waters within the mature anticyclonic eddy which were characteristic of the APFZ have been modified during this eddy's displacement south. These stations, within the mature anticyclonic eddy, particularly the grey and magenta profiles, depict the severe interleaving present at the circumference of the mature anticyclonic eddy. These 6 profiles are dissimilar to the 4 station profiles seen within the juvenile anticyclonic eddy [Figure 26], seen there to be smoother.

4.3.3 - OVERVIEW OF THE HYDROGRAPHICAL ANALYSIS

THERMAL STRUCTURE

When comparing the temperature sections of the juvenile and mature anticyclonic eddies, it can be seen that a loss of temperature occurs during the southward propagation of a mature eddy. The temperatures of the juvenile eddy, a proptotype for anticyclonic eddies created by the SWIR, appear to range from 4.5°C at the surface with internal temperatures decreasing to 2.5°C. In comparison, the mature eddy has surface and internal temperatures of 1.75°C, which are expected within anticyclonic mesoscale feature. However, since the exterior profiles are comparitively cooler [by ±2°C], this mature eddy has brought atypical water south into this region of the ACC. Atypical water with lower surface salinities, but more importantly, warmer subsurface temperatures. It is therefore surmised that, with maturity, the bulk of the heat within the anticyclonic eddy sinks, involving a relative cooling at the surface of the advecting eddy. What was noted was that there is a major difference in the depth of the Antarctic Intermediate Water mass [AAIW] between the two eddies [Figures 26, 28 and 30]. Park et al. (1997) explained that the waters typical of this region of the AAZ, with the associated WW, formed south of the APF, typically consisted of a shallow

temperature minimum of <-0.3 °C, at approximately 100m. Whereas, observed within the anticyclonic eddies, particularly the mature feature, were waters typical of modified APFZ, with a subsurface temperature maximum (Park et al., 1997).

Past literature has reported that the average depth of mesoscale eddies is 1000m (Wang et al., 2003; Ansorge et al., 2005), while Durgadoo et al. (2011) observed cyclonic eddies, forming as a result of the South West Indian Ridge [SWIR], with depths between 2000 and 3000m. From the thermal sections of the two profiled anticyclonic eddies, their depth range was found to lie between 1200 – 1500m.

SALINITY STRUCTURE

By comparing the salinity sections of the juvenile and mature anticyclonic eddies, the clearest difference is in the depths of the stratification. The stratification of the juvenile eddy extended to a depth of 1200m, whereas the mature eddy's stratification was confined in the top 300m. The juvenile salinity section shows the early conditions within the eddy, whereas the mature section represents the eddy's conditions after time has passed and passage has occurred. It is therefore surmised that, with maturity, the stratification within the eddy becomes shallower and the pycnoclines become more regular. However, the surface pool of relatively low salinity water [<34psu] does not deepen significantly over time, but widens at the surface to span the entire eddy diameter. The surface salinity minimum typical of the APFZ, seen in the anticyclonic eddies of this area, are as a result of an abundant fresh water supply to the surface due to high rainfall typical of the Sub-Antarctic Polar Frontal Zone [SAPFZ]. This is the reason why the eddies of this area have a surface layering of fresh water overlying a subsurface salinity maximum.

WATER MASS COMPARISON

Increasing eddy age has also caused a deterioration of water mass boundary strength: this can be seen from the temperature/salinity plots, where there is a severe amount of water mass interleaving at the edge of the mature anticyclonic eddy. A cause for this interleaving of water mass boundaries, is likely to be the vertical current shear associated with the rotational nature and baroclinic situation of the mesoscale eddies themselves as they are ''spinning down" (Bakun A., 2006). With the presence of interleaving, property transfer appears to increase as the eddy ages and advects south. Furthermore, with the scale of interleaving increasing, there would be an acceleration of this transfer of properties. In this way, as the anticyclonic eddy ages, the heat and salt fluxes at its water mass boundaries accelerate over time. Eddy decay or modification may also have been as a result of air-sea interactions at this location [evident from the surface characteristic differences between the juvenile and mature eddy] or the subsurface interactions due to intrusions of surrounding waters [interleaving].

5 - CONCLUSION

Past investigations (Gouretski and Danilov 1994; Ansorge et al., 2015) have identified a southerly extension of sea surface variability, extending southwards from the Andrew Bain Fracture Zone section [ABFZ] of the South West Indian Ridge [SWIR]. These very same studies identified that a mesoscale eddy corridor were created by a series of anticyclonic eddies, which advected across the Antarctic Circumpolar Current [ACC]. Prior to Ansorge et al. (2015) previous studies of this area of high mesoscale activity were carried out over two decades ago. In order to better understand the characteristics of these anticyclonic mesoscale eddies which travel south, an in depth analysis using up-to-date sampling equipment and improved techniques was required. Using two satellite-based datasets and in situ measurements, this thesis aimed at establishing an understanding of where and how these features advect, and to determine their recent hydrographic structure.

OBJECTIVE 1 - Establish a more in depth analysis of this southerly extension of sea surface variability, by performing a more thorough assessment of the recent eddy dynamics within.

OBJECTIVE 2 - Investigate the historical dynamics which occurred within the southward anticyclonic mesoscale eddy corridor.

OBJECTIVE 3 - Sample and compare the hydrographical structure of two particular anticyclonic mesoscale eddies within the southward extending anticyclonic mesoscale eddy corridor.

5.1 - ARE THERE MESOSCALE EDDIES TRAVELLING SOUTHWARDS FROM THE SWIR?

The first objective intended to answer the key question of whether or not there are mesoscale eddies travelling southwards from the SWIR. A contemporary Hovmöller analysis of the southward propagation of anticyclonic mesoscale eddies across the entire eddy hotspot [Figures 5 and 7], showed an average rate of 7 eddies per year to have shifted south through the southward extending anticyclonic mesoscale eddy corridor between 2012 and 2014. A result which differs to the rate from the Chelton et al. (2011) data set analysis due to differing methodologies: a temporally uninterrupted hovmöller analysis as opposed to a tracking scheme with weekly time steps and the potential for smaller features to have been unobserved.

A high proportion of the southward anticyclonic mesoscale eddies appeared to have been shed from a 'quasi permanent' anticyclonic feature, typically present between 49° and 50˚S. From this result it was surmised that the 'quasi permanent' anticyclonic feature acts as the southward shifting anticyclonic eddies' origin point, and is thought to be associated with the convergence of the Subantarctic Front [SAF] and the Antarctic Polar Front [APF] at the ABFZ (Ansorge and Lutjeharms, 2003). The southward advection of the relatively smaller anticyclonic eddies from this 'quasi-permanent' feature, could have occurred as a result of the southward deflection of the SAF and the APF downstream of the SWIR. This objective's Hovmöller

analysis also shows confirmation that the ABFZ was the point of origin for the two anticyclonic eddies which were sampled and investigated by the in situ analysis in Objective 3.

5.2 - WHAT ARE THE TRACK CHARACTERISTICS OF THE SOUTHWARD MOVING EDDIES?

The second objective intended to answer the key question of determining the track characteristics of the southward propagating mesoscale eddies. From the historical track survey of 1992 - 2012, 25 particular eddies generally followed the southern slope of the SWIR, with an area of track constriction at ±28°E, 52°S, south of which the eddy pathways spread out. The majority of these features lasted for 25 weeks, with one lasting longer than 55 weeks. It also appeared that most tracks dissipated by 55°S regardless of their age. The scalar analysis of these twenty five southward propagating eddies, showed that after 12 weeks they exhibited, on average; non-linear shrinking of radii, an irregular weakening in circum-average speed and a slow decline in Sea Surface Height. With the laws of conserving potential vorticity, it can be surmised that the depth of the features, which are destined to shift southwards, may be a deciding factor influencing the traits of their future trajectory. Due to the high variability of the fronts of the ACC, and their specific jet strengths, they are likely to have an influence on the anticyclonic eddy tracks' directionality. Furthermore, as the average radii of these features are significantly larger than the first baroclinic Rossby radius of deformation in the area [10-20km] (Chelton et al., 1998), what governs the size of these features?

5.3 - HOW ARE THESE MESOSCALE FEATURES STRUCTURED HYDROGRAPHICALLY?

The third objective intended to answer the key question regarding the determination of the hydrographic structure of anticyclonic eddies found within the eddy corridor. From this study's hydrographical comparison of the juvenile and mature mesoscale eddies, it is apparent that, during the displacement south of the mesoscale eddy through the anticyclonic mesoscale eddy corridor, it was seen that hydrographic fluctuations were experienced. The mature anticyclonic feature, compared to the juvenile feature, shows a deepening to over 1300m during its displacement south, with an internal [subsurface] maximum temperature decrease of 0.4°C. Other hydrographic structural differences are that the mature feature contains the majority of its heat in a subsurface core and has a stratified salinity profile, whereas the juvenile feature stores most of its heat at the surface and has a low surface salinity layer, both above 200m. This analysis of in situ data of each of the two profiled eddies propagating southward from the SWIR, showed similar layering of water masses within. However, it was noted that there was a major difference in the depth of the Antarctic Intermediate Water mass between the two eddies. This implies that AAIW was the most responsive of all the contained water masses, with regards to travelling time and eddy dynamics. When comparing the temperature sections between the mature and juvenile anticyclonic eddies, a significant loss of heat was shown to have occurred during the southward propagation of the mature eddy. Increasing age had appeared to have caused a deterioration of water mass boundary strength: the temperature/salinity plots show there was severe water mass interleaving at the edge of the mature anticyclonic eddy allowing for water property transfer. So it has been determined that 'aging', as a

result of geographic displacement, has an influence on the structural integrity of the southward propagating eddies as well as on the hydrographical content of the surrounding host waters. Therefore, oceanographically, southward propagating anticyclonic mesoscale eddies act as vehicles relocating water masses typical of the Antarctic Polar Frontal Zone [APFZ] southwards into the Antarctic Zone.

5.4 - LIMITATIONS AND FUTURE RECOMMENDATIONS

This study is the first focussed and in depth study of the eddies which are known to relocate southwards through the southward extending eddy corridor as confirmed in Ansorge et al. (2015). Since the results of this study seem significant due to the role that mesoscale eddies have in relocating warmer water masses across the ACC, it is hoped that it will encourage more ship time to be dedicated to monitor these transported waters. This would allow for a more thorough understanding of the impacts this corridor has on the present day surrounding environment and to the future impacts this corridor could have on climate change.

Limitations of this study were the shortcomings of the Chelton et al. (2011) data set, which promote the need for future surveys of the southward anticyclonic corridor to be based on SSH data which accurately detects the authentic eddy populations of the area, merged with, as mentioned above, an improved knowledge of hydrographic detail. Further limitations, for the in situ study were due to the lack of ship time made available for the in situ survey of the 2 anticyclonic mesoscale eddies, resulting in only 3 transects and an increase in spatial resolution between consecutive Expendable Bathythermograph and Conductivity, Temperature and Depth stations along each transect. The wide distances between sampling stations, along with the lack of multiple transects across the 2 anticyclonic eddies, as well as the reduced scientific capabilities of the SA Agulhas II in highly rough seas, hampered the resolution and comprehensiveness of the hydrographic survey. Increased available ship time for annually repeated transects across the southward propagating SWIR eddies, with stations closer than 32 nautical miles, will allow for a more comprehensive analysis of the corridor's heat and salt flux trends. With the presence of warmer water masses within the Southern Ocean, negative shifts in the uptake of CO_2 occur. Hence the southward train of anticyclonic [warm core] features, investigated by this thesis, has the potential of impacting the ability for this region of the SO to take up atmospheric CO_2. In order to make comparisons with other sectors of the SO, another hydrographic variable which would be beneficial to measure during future in situ analyses, is the CO_2 levels of this region south of the SWIR.

Other recommendations for useful future research into this area of study, using future in situ measured data, are to include density signatures in hydrographical sections to improve the water mass distinction and also to perform calculations of heat fluxes across water mass boundaries. An update and the continued validation of the Chelton et al. (2011) dataset would be most beneficial for future altimetry based research.

The results of this study of the SWIR eddies are the first of its kind and could hopefully be a catalyst for future research in this area. Knowledge of the detailed contents of these mesoscale eddies is critical, as they have a significant affect on the heat and salt content of the SO which subsequently impacts the ventilation of the Meridional Overturning Circulation by altering the hydrographic makeup of water masses such as the seasonal distribution of Winter Water. These eddies also have the power to alter the SO's CO_2 absorption/production capabilities. As this carbon sink is vitally important with regards to climate change, the quantification of the heat and salt sources of the SO, which alter the SO's ability to absorb CO_2, is imperative.

APPENDIX A – EXPANDED VERSION OF FIGURE 5

The temporal sea surface height standard deviation from satellite altimetry data for the period 1993 - 2009. The area of high mesoscale activity, south of the South-West Indian Ridge, is shown enclosed by a dashed white line. Red to yellow areas signify areas of high sea surface variability, while green to blue areas signify regions of low sea surface variability. Image provided courtesy of Sam Ebernez, GEOMAR, Helmholtz Centre for Ocean Research.

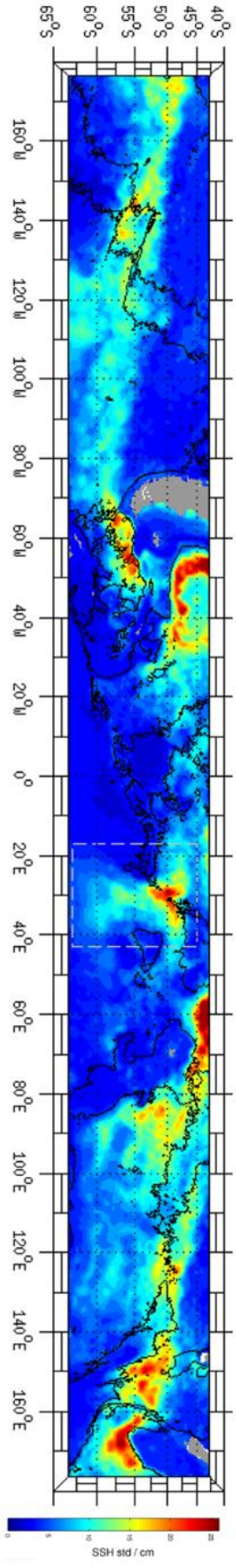

APPENDIX B – TRAJECTORY PLOTS

Individual trajectory plots of the anticyclonic mesoscale eddies which were found to propagate south by Ansorge et al. (2014). The eddy identity number is listed in the title of each trajectory plot. Bathymetric environment is shown with the 3500m isobaths [shown with black line]. A single trajectory consists of a starting position [demarcated with a red 'o'], a red track line and the termination position [symbolised by a red 'x'].

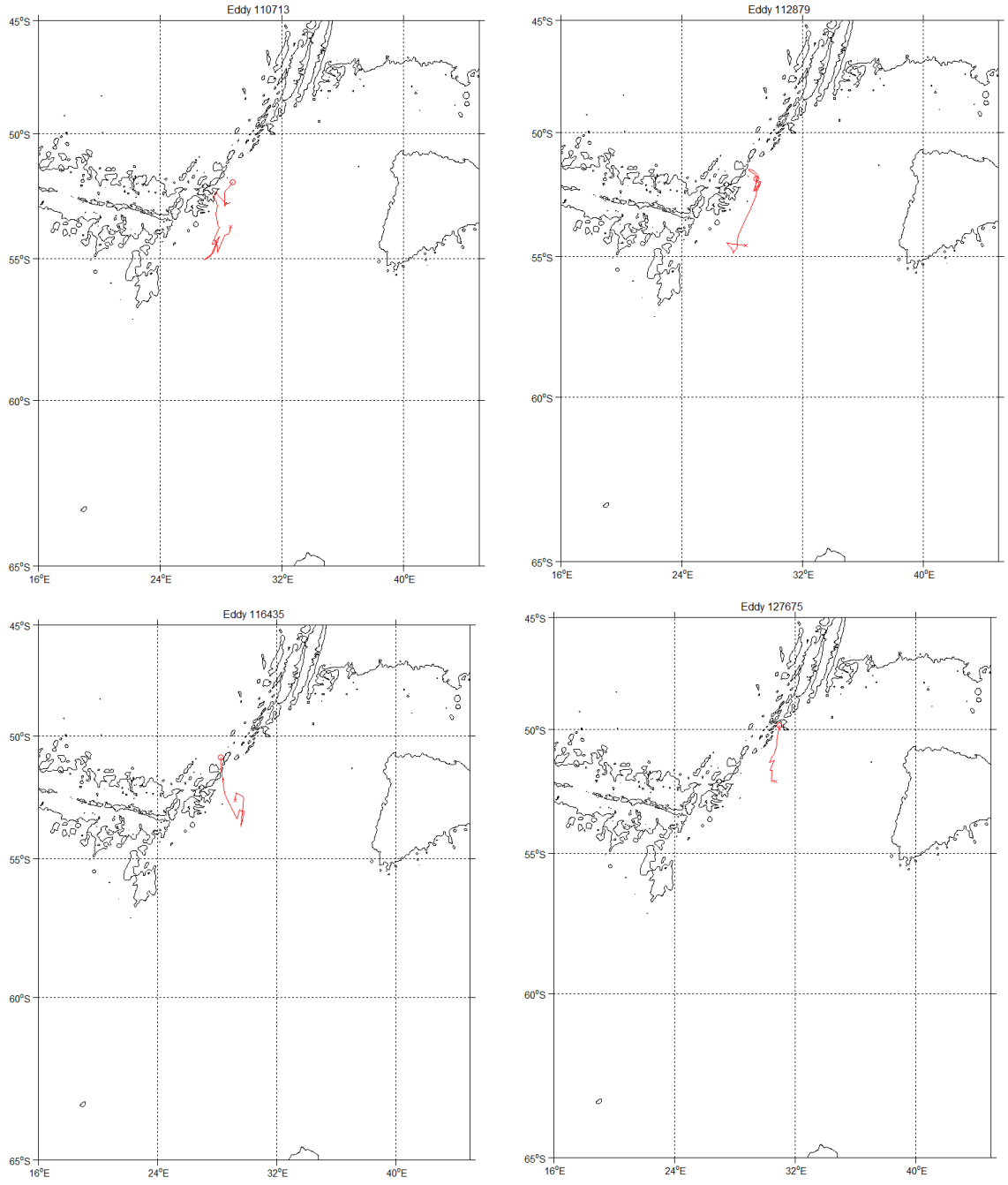

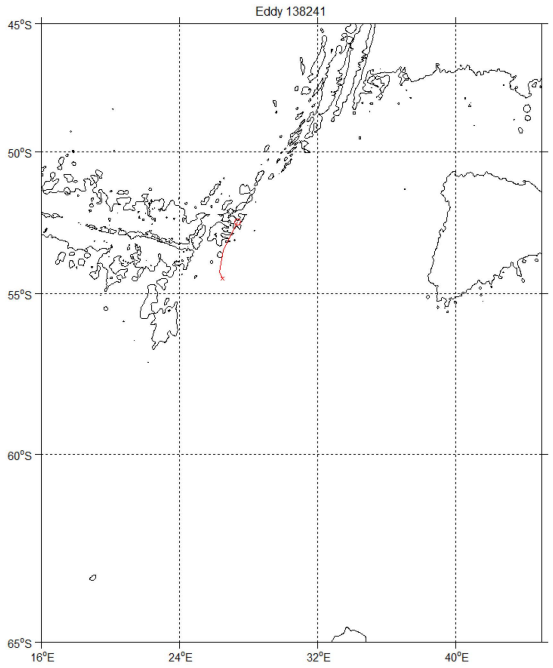
Eddy 138241
45°S
50°S
55°S
60°S
65°S
16°E
24°E
32°E
40°E

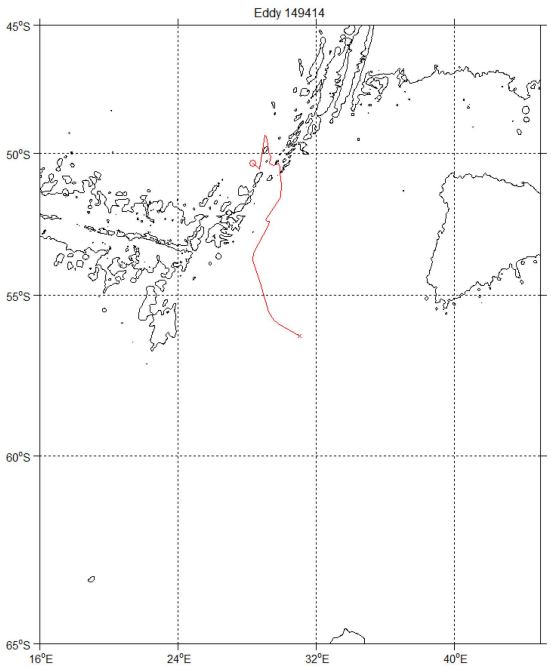
Eddy 149414
45°S
50°S
55°S
60°S
65°S
16°E
24°E
32°E
40°E

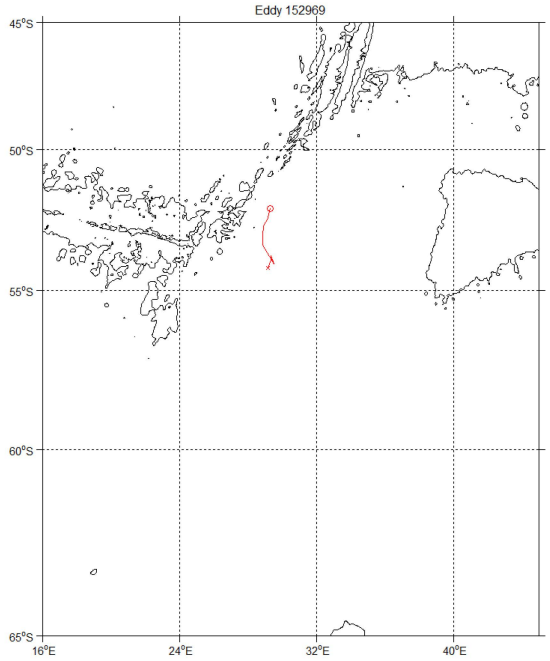
Eddy 152969
45°S
50°S
55°S
60°S
65°S
16°E
24°E
32°E
40°E

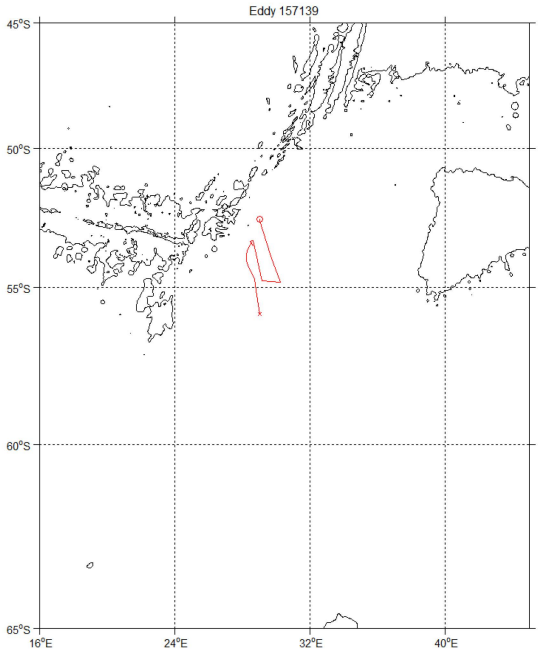
Eddy 157139
45°S
50°S
55°S
60°S
65°S
16°E
24°E
32°E
40°E

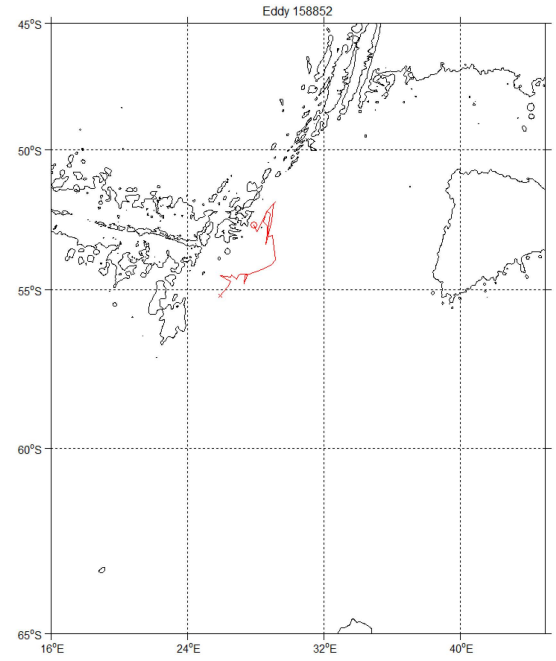
Eddy 158852
45°S
50°S
55°S
60°S
65°S
16°E
24°E
32°E
40°E

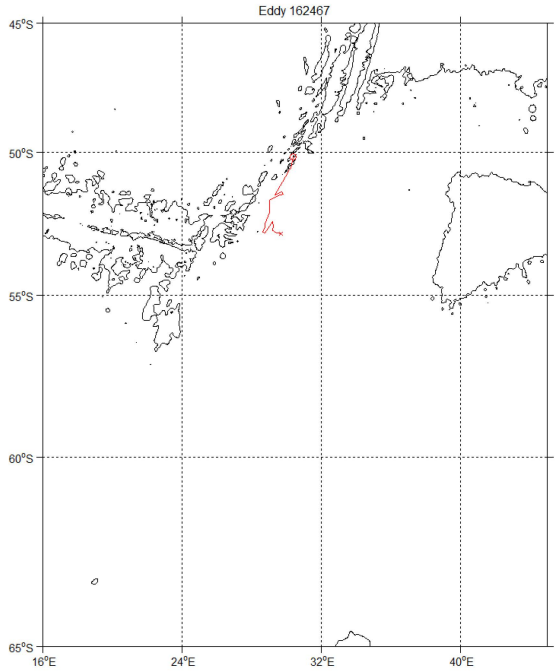
Eddy 162467
45°S
50°S
55°S
60°S
65°S
16°E
24°E
32°E
40°E

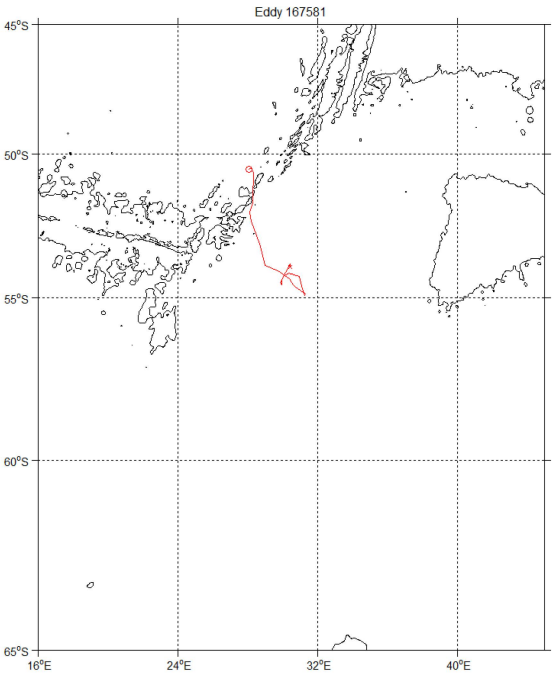
Eddy 167581
45°S
50°S
55°S
60°S
65°S
16°E
24°E
32°E
40°E

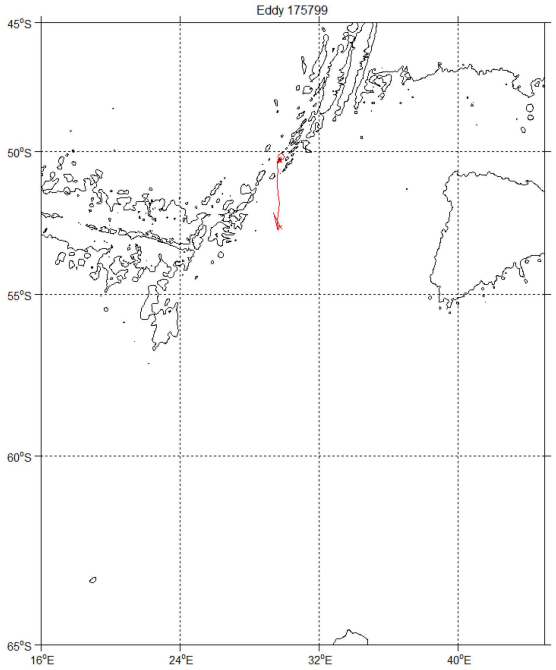
Eddy 175799
45°S
50°S
55°S
60°S
65°S
16°E
24°E
32°E
40°E

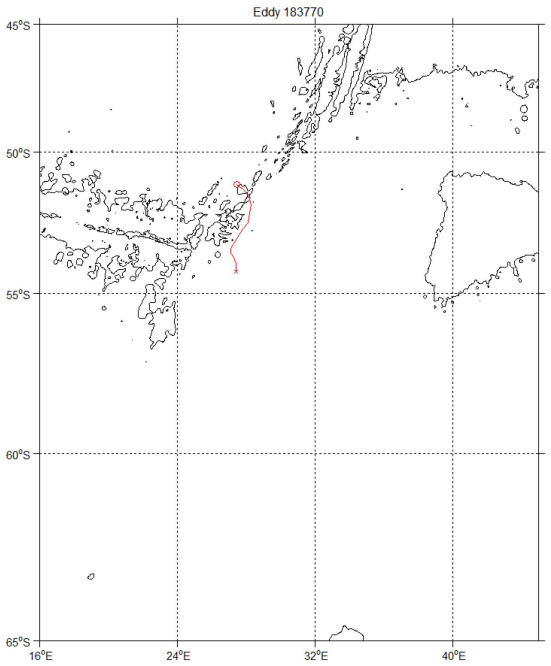
Eddy 183770
45°S
50°S
55°S
60°S
65°S
16°E
24°E
32°E
40°E

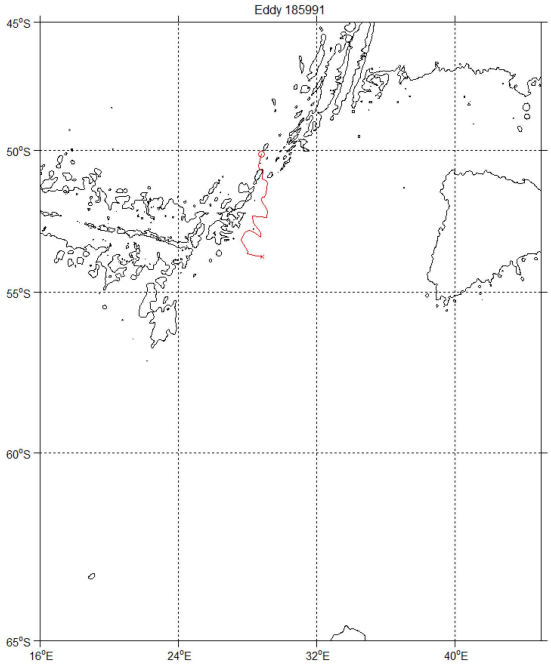
Eddy 185991
45°S
50°S
55°S
60°S
65°S
16°E
24°E
32°E
40°E

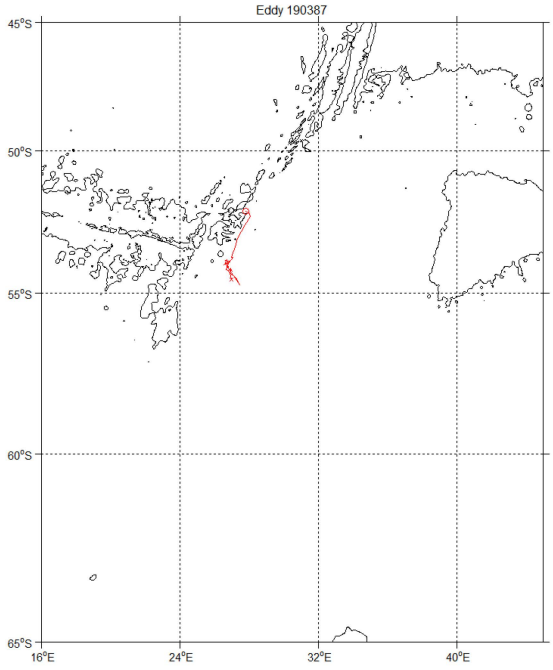
Eddy 190387
45°S
50°S
55°S
60°S
65°S
16°E
24°E
32°E
40°E

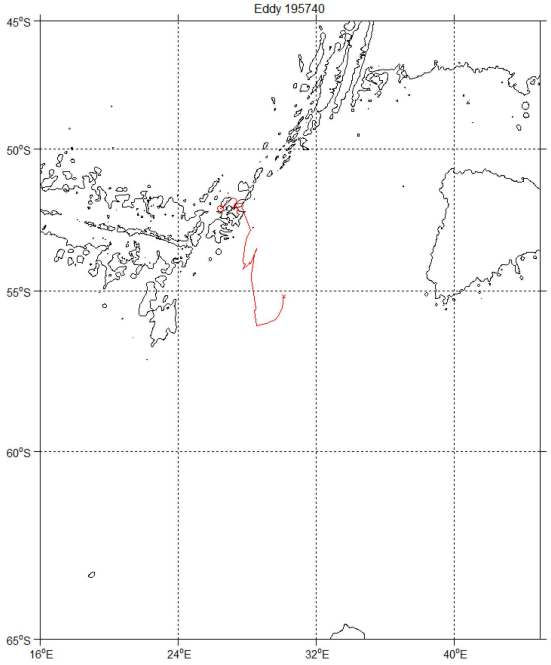
Eddy 195740
45°S
50°S
55°S
60°S
65°S
16°E
24°E
32°E
40°E

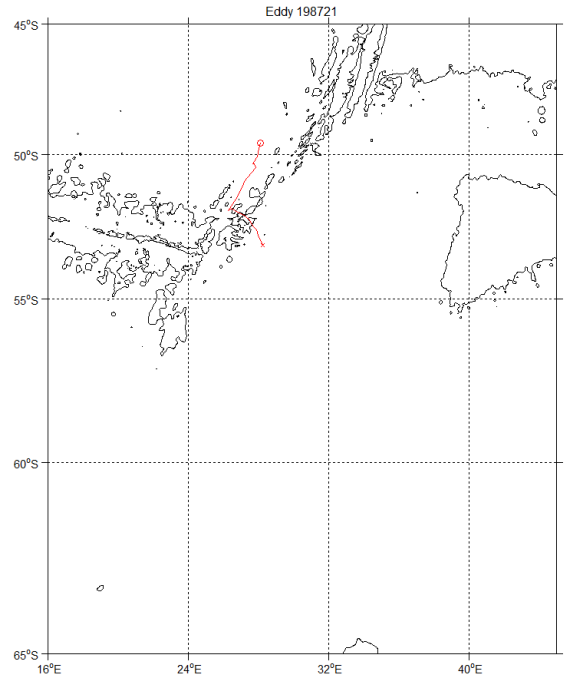
Eddy 198721
45°S
50°S
55°S
60°S
65°S
16°E
24°E
32°E
40°E

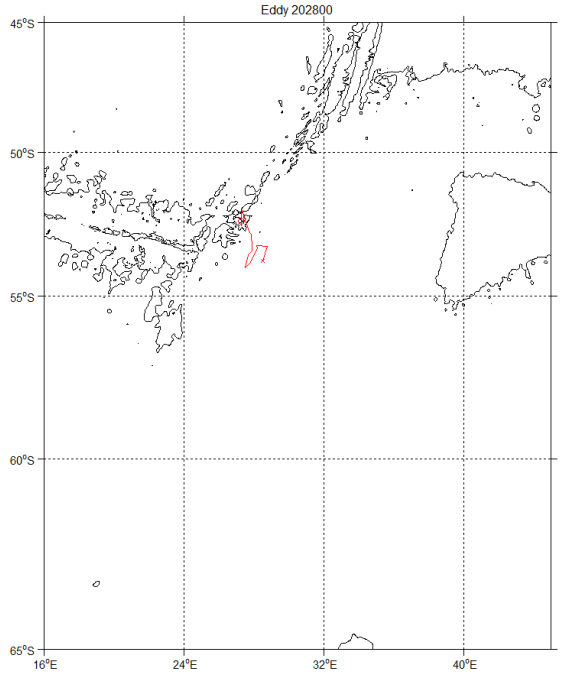
Eddy 202800
45°S
50°S
55°S
60°S
65°S
16°E
24°E
32°E
40°E

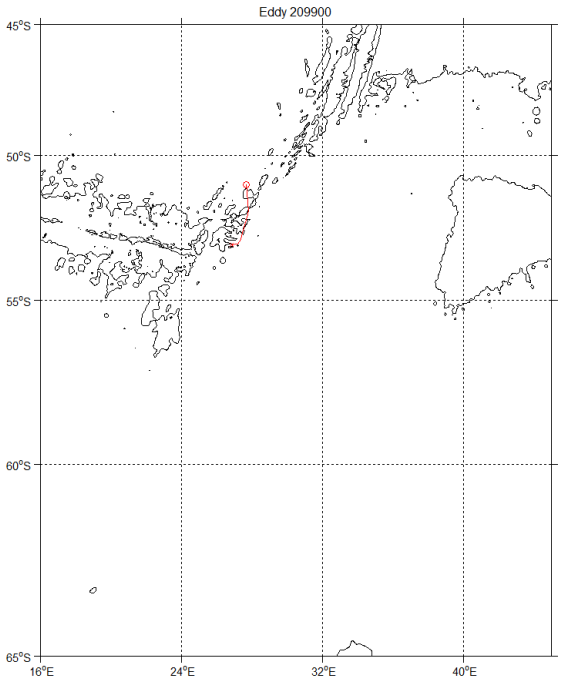
Eddy 209900
45°S
50°S
55°S
60°S
65°S
16°E
24°E
32°E
40°E

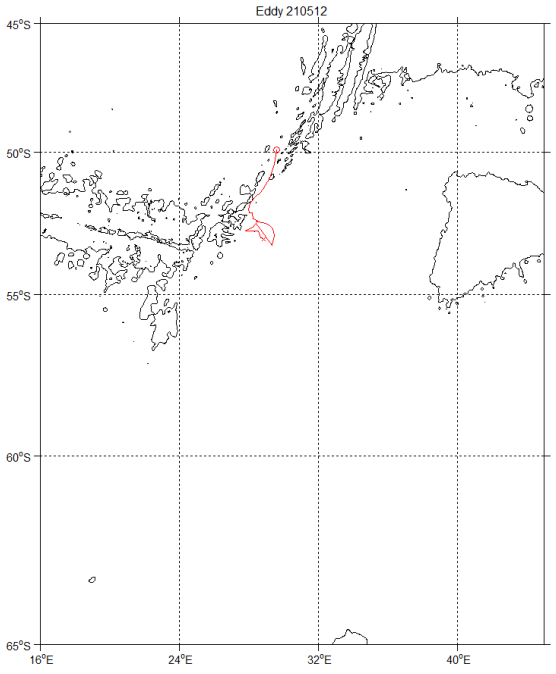
Eddy 210512
45°S
50°S
55°S
60°S
65°S
16°E
24°E
32°E
40°E

APPENDIX C – THE 25 EDDIES SOURCED FROM CHELTON et al. (2011)

IDENTITY NUMBER	TOTAL SAMPLING INTERVALS [7 day time step]
110713	33
112879	32
116435	18
127675	13
138241	4
149414	29
152969	10
157139	19
158852	38
159817	25
162467	23
167581	30
175799	20
180229	30
183770	16
184852	17
185991	33
188503	35
190387	33
191298	37
195740	58
198721	27
202800	21
209900	10
210512	27

APPENDIX D – GLOSSARY

Acronyms are listed in alphabetical order.

ACRONYM	IN FULL
AABW	Antarctic Bottom Water
AAIW	Antarctic Intermediate Water
ABFZ	Andrew Bain Fracture Zone
ACC	Antarctic Circumpolar Current
ADCP	Acoustic Doppler Current Profiler
APF	Antarctic Polar Front
ASF	Antarctic Slope Front
AAZ	Antarctic Zone
CDW	Circumpolar Deep Water
CO_2	Carbon Dioxide
CTD	Conductivity, Temperature & Depth
DEIMEC 1	Dynamics of Eddy Impacts on Marion's Ecosystem 1
ETOPO2	Earth Topography Version 2
ETOPO2V2C	Earth Topography Version 2 Centred Cell
MADT	Delayed Time Absolute Dynamic Topography
MIRC2014	Marion Island Relief Cruise 2014
MOC	Meridional Overturning Circulation
M-SASW	Moderated Sub-Antarctic Surface Water
NOAA	National Oceanic and Atmospheric Administration
NRF	National Research Fund
PEI	Prince Edward Island
PFZ	Polar Frontal Zone
PSU	Practical Salinity Units
SACCF	Southern boundary front of the Antarctic Circumpolar Current
SAF	Sub-Antarctic Front
SANAP	South African National Antarctic Program
SAPFZ	Sub-Antarctic Polar Frontal Zone
SASW	Sub-Antarctic Surface Water
SB	Southern Boundary Current
SBE	Sea-Bird Electronics
SO	Southern Ocean
SPZ	Subpolar Zone
SSH	Sea Surface Height
SSHA	Sea Surface Height Anomaly
STF	Sub-Tropical Front
Sv	Sverdrup
SWINDEX	South-West Indian Ocean Experiment
SWIR	South West Indian Ridge
SZ	Southern Zone
T/S	Temperature/Salinity
UCT	University of Cape Town
WW	Winter Water
XBT	Expendable Bathythermograph

APPENDIX E - REFERENCES

JOURNAL ARTICLES:

Ansorge, I. J., & Lutjeharms, J. R. E., 2003. Eddies originating from the South-West Indian Ridge. *Journal of Marine Systems, 39*, 1-18. doi:10.1016/S0924-7963(02)00243-9

Ansorge, I. J., & Lutjeharms, J. R. E., 2005. Direct observations of eddy turbulence at a ridge in the Southern Ocean. *Geophysical Research Letters, 32*, L14603. doi:10.1029/2005GL022588

Ansorge, I. J., Lutjeharms, J. R. E., Swart, N. C., & Durgadoo, J. V., 2006. Observational evidence for a cross frontal heat pump in the Southern Ocean. *Geophysical Research Letters,* 33, L19601. doi:10.1029/2006GL026174

Ansorge, I. J., Jackson, J., Reid, K., Durgadoo, J. V., Swart, S., & Eberenz, S. (2014). Evidence of a southward eddy corridor along the South-West Indian Ocean. *Deep-Sea Research II*, 119, 69-76. doi:10.1016/j.dsr2.2014.05.012

Bakun, A. (2006). Fronts and eddies as key structures in the habitat of marine fish larvae: opportunity, adaptive response and competitive advantage. *Scientia Marina, 70S2,* 105-1122.

Budillon, G., & Rintoul, S.R. (2003). Fronts and upper ocean thermal vaiability south of New Zealand. *Arctic Science, 15*, 141-152.

Bryden, H. L., & Heath, R. A. (1985). Energetic eddies at the northern edge of the Antarctic Circumpolar Current in the southwest Pacific. Progress in Oceanography, 14, 65–87.

Chelton, D. B., Deszoeke, R. A., Schlax, M. G., El Naggar, K., & Siwertz, N. (1998). Geographical variability of the first baroclinic Rossby radius of deformation. *Journal of Physical Oceanography*, 28(3), 433-460.

Chelton, D. B., Schlax, M. G., & Samelson, R. M. (2011). Global observations of nonlinear mesoscale eddies. *Progress in Oceanography, 91*, 167-216. doi:10.1016/j.p.ocean.2011.01.002

Craneguy P., and Park Y.-H., 1999. Topographic control of the Antarctic circumpolar current in the Soith Indian Ocean. *Compte Rendu Academie Scientific*. Paris, 328, 583-589.

Durgadoo, J. V., Lutjeharms, J. R. E., Baistoch, A., & Ansorge, I. J. (2008). The Conrad Rise as an obstruction to the Antarctic Circumpolar Current. *Geophysical Research Letters, 35*, L20606. doi:10.1029/2008GL035382

Durgadoo, J. V., Ansorge, I. A., & Lutjeharms, J. R. E. (2010). Review oceanographic observations of eddies impacting the Prince Edward Islands, South Africa. *Antarctic Science, 22(3)*, 211-219. doi:10.1017/S0954102010000088

Durgadoo, J. V., Ansorge, I. J., de Cuevas, B. A., Lutjeharms, J. R. E., Coward, A. C. (2011). Decay of eddies at the South-West Indian Ridge. *South African Journal of Science,* 107(11/12), 1-10.

Firing, Y. L., Chereskin, T. K., & Malzoff, M. R. (2011). Vertical structure and transport of the Antarctic Circumpolar Current in Drake Passage from direct velocity observations. *Journal of Geophysical Research, 116*, C08015. doi:10.1029/2011JC006999

Gille, S. T. (1997). The Southern Ocean Momentum Balance: Evidence for Topographic Effects from Numerical Model Output and Altimeter Data. *Journal of Physical Oceanography, 27*, 2219-2232.

Gille, S. T. (2002). Float Observations of the Southern Ocean. Part I: Estimating Mean Fields, Bottom Velocities and Topographic Steering. *Journal of Physical Oceanography, 33*, 1167-1181.

Gordon, A. L., Molinelli, E., & Baker T. (1978). Large-Scale Relative Dynamic Topography of the Southern Ocean. *Journal of Geophysical Research,* 83, 3023-3032.

Gouretski, V. V., & Danilov, A. I. (1993). Weddell Gyre: structure of the eastern boundary. *Deep-Sea Research I,* 40(3), 561-582. doi:10.1016/0967-0637(93)90146-T

Gouretski, V. V., & Danilov, A. I. (1994). Characteristics of warm rings in the African sector of the Antarctic Circumpolar Current. *Deep-Sea Research I, 41(8)*, 1131-1157. doi:10.1016/0967-0637(94)90037-X

Hofmann, E. E. (1985). The large-scale horizontal structure of the Antarctic Circumpolar Current from FGGE drifters. *Journal of Geophysical Research: Oceans*, *90*(C4), 7087-7097.

Hogg, A. M. (2010). An Antarctic Circumpolar Current driven by surface buoyancy forcing. *Geophysical Research Letters*, 37, L23601. doi:10.1029/2010GL044777

Hughes, C. H., & Ash, E. R. (2001). Eddy forcing of the mean flow in the Southern Ocean. *Journal of Geophysical Research, 106(C2),* 2713-2722. doi:10.1029/2000JC900332

Hughes, C. W. (2005). Nonlinear vorticity balance of the Antarctic Circumpolar Current. *Journal of Geophysical Research: Oceans, 110*(C11).

Ito, Woloszyn & Mazloff, (2010). Anthropogenic carbon dioxide transport in the Southern Ocean driven by Ekman flow. *Nature,* 463, 80-84. doi:10.1038/nature08687

Iudicone, D., Speich, S., Madec, G., & Blanke, B. (2008). The global conveyor belt from a Southern Ocean perspective. *Journal of Physical Oceanography*, *38*(7), 1401-1425.

Lenn, Y., Chereskin, T. K., Sprintall, J., & Firing, E. (2007). Mean jets, mesoscale variability and eddy momentum fluxes in the surface layer of the Antarctic Circumpolar Current in the Drake Passage. *Journal of Marine Research, 65*, 27-58.

Lumpkin, R., & Speer K. (2006). Global Ocean Meridional Overturning. *Journal of Physical Oceanography, 37*, 2550 – 2562.

Lutjeharms, J. R. E., & Baker, D. J. (1980). A statistical analysis of the meso-scale dynamics of the Southern Ocean. *Deep-Sea Research A: Oceanographic Research Papers, 27,* 145-159.

Moore, J. K., Abbott, M. R., & Richman, J. G. (1999). Location and dynamics of the Antarctic Polar Front from satellite sea surface temperature data. *Journal of Geophysical Research: Oceans*, *104*(C2), 3059-3073.

Niiler, P. P., Maximenko, N. A., & McWilliams, J. C. (2003). Dynamically balanced absolute sea level of the global ocean derived from near-surface velocity observations. *Geophysical Research Letters*, 30, 2164. doi:10.1029/2003GL0186282

Orsi, A. H., Whitworth, T., & Nowlin, W. D. (1995). On the meridional extent and fronts of the Antarctic Circumpolar Current. *Deep Sea Research I, 42(5),* 641-673. doi:10.1016/0967-0637(95)00021-W

Park, Y.-H., Charriaud, E., & Fieux, M. (1997). Thermohaline Structure of the Antarctic Surface Water/Winter Water in the Indian Sector of the Southern Ocean. *Journal of Marine Science, 17*, 5-23.

Park, Y.-H., E. Charriaud, P. Craneguy, and A. Kartavtseff (2001), Fronts, transport, and Weddell Gyre at 30°E between Africa and Antarctica, *Journal of Geophysical Research: Oceans,* 106(C2), 2857–2879, doi:10.1029/2000JC900087.

Pollard, R. T., & Read, J. F. (2001). Circulation pathways and transports of the Southern Ocean in the vicinity of the Southwest Indian Ridge. *Journal of Geophysical Research: Oceans*, 106(C2), 2881-2898..

Roquet, F., Park, Y., Guinet, C., Bailleul, F., & Charrassin, J., 2009. Observation of the Fawn Trough Current over the Keregulen Plateau from instrumented Elephant seals. *Journal of Marine Science*, 78, 377-393. doi:10.1016/j.jmarsys.2008.11017

Sangrà, P., Pelegrí, J. L., Hernández-Guerra, A., Arregui, I., Martín, J. M., Marrero-Díaz, A., Martínez, A., Ratsimandresey, A. W., & Rodríguez-Santana, A. (2005). Life history of an anticyclonic eddy. *Journal* of *Geophysical Research: Oceans,* 110(C3).

Sandwell, D. T., & Zhang, B. (1989). Global mesoscale variability from the Geosat exact repeat mission: Correlation with ocean depth. *Journal of Geophysical Research: Oceans*, 94(C12), 17971-17984.

Sclater, J. G., Grindlay, N. R., Madsen, J. A., & Rommevaux-Jestin, C. (2005), Tectonic interpretation of the Andrew Bain transform fault: Southwest Indian Ocean. *Geochemical, Geophysical, Geosystems, 6*, Q09K10, doi:10.1029/2005GC000951.

Schröder, M., & Fahrbach, E. (1999). On the structure and the transport of the eastern Weddell Gyre. *Deep Sea Research II: Topical Studies in Oceanography*, *46*(1), 501-527.

Sloyan, B. M., & Rintoul, S. R. (2001). The southern ocean limb of the global deep overturning circulation*. *Journal of Physical Oceanography*, *31*(1), 143-173.

Sokolov, S., & Rintoul, S. R. (2002). Structure of Southern Ocean fronts at 140°E. *Journal of Marine Systems*, *37*(1), 151-184.

Sokolov, S., & Rintoul, S. R. (2007). Multiple jets of the Antarctic Circumpolar Current south of Australia*. *Journal of Physical Oceanography*, *37*(5), 1394-1412.

Sokolov, S., & Rintoul, S.R., 2009. Circumpolar structure and distribution of the Antarctic Circumpolar Current fronts: 1. Mean circumpolar paths. *Journal of Geophysical Research, 114*, C11018. doi:10.1029/2008JC005108.

Sutyrin, G. G., Rowe, G. D., Rothstein, L. M., & Ginis, I. (2003). Baroclinic eddy interactions with continental slopes and shelves. *Journal of physical Oceanography*, *33*(1), 283-291.

Sutyrin, G., Stegner, A., Taupier-Letage, I., & Teinturier, S. (2009). Amplification of a surface-intensified eddy drift along a steep shelf in the Eastern Mediterranean Sea. *Journal of Physical Oceanography*, *39*(7), 1729-1741.

Trenberth, K. E., Large, W. G., & Olson, J. G. (1990). The mean annual cycle in global ocean wind stress. *Journal of Physical Oceanography*, 20(11), 1742-1760.

Wang G., Su J., & Chu P. C., 2003. Mesoscale Eddies In The South China Sea Observed With Altimeter Data. *Geophysical Research Letters, 30(21),* 2121. doi:10.1029/2003GL018532

White, W. B., & Peterson, R. G. (1996). An Antarctic circumpolar wave in surface pressure, wind, temperature and sea-ice extent. *Nature*, *380*(6576), 699-702.

BOOKS:

Pedlosky, J. (2013). Ocean circulation theory. Springer-Verlag, New York, pp. 453. ISBN-13 978-0-387-6387-7

Rintoul, S. R., & Naveira Garabato, A. C. (2013). Dynamics of the Southern Ocean Circulation, Ocean Circulation and Climate - A 21st Century Perspective, Elsevier BV, G Siedler, SM Griffies, J Gould and JA Church (ed), United Kingdom, pp. 471-492. ISBN 978-0-12-391851-2

Talley, L. D. Pickard, G. L. Emery, W. J. Swift, J. H. (2011). Descriptive physical oceanography: an introduction: Sixth Edition. Academic Press, Amsterdam, VIII, pp. 555. ISBN 9780750645522

IMAGES:

Figure 4:
The mesoscale ocean circulation [lyapunov exponents] around Antarctica for 27 May, 2014. The altimeter product produced by *Ssalto/Duacs* in collaboration with LOcean and *CTOH* and distributed by *Aviso*, with support from *Cnes* (http://www.aviso.altimetry.fr/).

Figure 5:
Temporal sea surface height standard deviation from satellite altimetry data for the period 1993-2009, provided courtesy of Sam Ebernez, GEOMAR, Helmholtz Centre for Ocean Research, Düsternbrooker Weg 20, 24105, Kiel, Germany.

PROGRAMS:

GEBCO - The bathymetry is reproduced from GEBCO Sheet G.08 compiled by R.L. Fisher of the Scripps Institution of Oceanography and extracted from the GEBCO Digital Atlas published by the British Oceanographic Data Centre on behalf of the IOC and IHO, 2003'.

MATLAB and Statistics Toolbox Release 2012a, the MathWorks Inc., Natic, Massachusettes, United States.

Ocean Data View 4 - Schlitzer, R., Ocean Data View, http://odv.awi.de, 2007.

DATA SOURCES:

2014 Marion Island Relief Cruise

The Chelton et al., (2011) dataset used, was downloaded from: http://cioss.coas.oregonstate.edu/eddies/

The altimeter products were produced and distributed by *Aviso* (http://www.aviso.altimetry.fr/), as part of the Ssalto ground processing segment. The specific website used for accessing the data used in Objective 1 was: http://las.aviso.oceanobs.com/las/getUI.do

The bathymetry data were produced by the U.S. Department of Commerce, National Oceanic and Atmospheric Administration, National Geophysical Data Center, 2006. ***2-minute Gridded Global Relief Data [ETOPO2v2]*** **(**http://www.ngdc.noaa.gov/mgg/fliers/06mgg01.html)